

THE GEOLOGY OF THE EAST MARKOYE REGION IN THE OUDALAN-GOUROUOL GREENSTONE BELT, NORTH-EAST BURKINA FASO.



An Honours Thesis by Luke Peters (0704730N)

Supervisor - Prof. Kim Ncube-Hein



WAXI- West African Exploration Initiative
IXOA- L'Initiative d'Exploration Ouest Africaine



Abstract

The rocks of the Oudalan-Gourouol Greenstone Belt (OGGB) are largely made up of supracrustal, island-arc derived sediments including, but not limited to, thick greywacke sequences. These were deposited in a deltaic-shelf environment on the margin of a back-arc basin. The local stratigraphy has been constrained by facies variation determined by sedimentary features and differences in the depositional environment. Regional low-middle greenschist metamorphism is shown by the ubiquitous presence of chlorite, epidote and minor muscovite and is suggested to be a result of large TTG pluton emplacement that occurred syn-tectonically with the Eburnean Orogeny. This thesis proposes it is due to diastathermal metamorphism caused by back-arc extension and mantle upwelling. Contact metamorphism of the greywacke to hornblende-hornfels facies occurs within close proximity of the calc-alkaline dykes. The internal structure and sedimentary features were destroyed due to the increase in temperature. Two deformation events occurred, the Tangaeen Event (2170-2130 Ma) and the Eburnean Orogeny (2130-1980 Ma) that caused the rocks in the OGGB to be folded twice. The Ludovic Fault System was a result of compression during the Eburnean Orogeny and gave rise to N-S trending, dextral-reverse structures. Dilation of these structures occurred due to compression of the Eburnean Orogeny. Granodiorite and monzodiorite dykes that intruded the Palaeoproterozoic sedimentary rocks were emplaced pre-D1 and underwent deuteritic alteration. They contain large, euhedral plagioclase and altered clinopyroxene crystals surrounded by a groundmass of quartz and secondary, interstitial plagioclase. The high quartz content, approximately 80 %, in these dykes is due to crustal contamination during emplacement.

Table of Contents

1.0. Acknowledgments	3
2.0. Introduction	4
2.1. Preamble	4
2.2. Location and Physiography	5
2.3. Aims	7
2.4. Acronyms, Abbreviations and Standards	7
3.0. Literature Review/Regional Geology	8
3.1. Stratigraphy	8
3.2. Sedimentology	8
3.3. Intrusions	10
3.4. Regional Tectonics	10
3.5. General Metallogensis and Targeting Potential	11
4.0. Methodology	12
4.1. Field Methodology	12
4.2. Laboratory Methodology	13
4.3. Petrography	15
5.0. Lithologies	20
6.0. Structure and Metamorphism	28
7.0. Geochemistry of Igneous Rocks	31
8.0. Depositional Environment	36
9.0. Tectonic Setting	40
10.0. Discussion	41
11.0. Conclusions	50
12.0. References	51
13.0. Appendix	58

1.0. Acknowledgments

The author would like to thank WAXI (West African Exploration Initiative), the Amira Group and its sponsors , Asinne Tshibubudze for his guidance, Prof. K.A.A Ncube-Hein for supervising and overseeing this project and to the staff of the Earth Lab at the University of the Witwatersrand.

Sponsors and research partners of the Amira Group:



2.0. Introduction

2.1. Preamble

The study area is situated in the Oudalan-Gourouol Greenstone Belt (OGGB) in north-east Burkina Faso (Fig. 1). Besides the research completed by Tshibubudze et al. (2009) which only encompassed a minor portion to the north of the study area, the study area has not been previously mapped or described. It therefore lacked any detailed geological interpretation. Hein et al. (2004), Tshibubudze et al. (2009) and Hein (2010) all referred to the controversy of stratigraphic “way up” in the West African Craton (WAC). Hirdes et al. (1996) concluded that the upper sequence of the Birimian is younger than the lower, whilst Milesi et al. (1991) stated the converse. However, Milesi et al. (1989) in Hirdes et al. (1996) originally agreed with the upper sequence being younger. Milesi et al. (1989) in Bossiere et al. (1996) also considered that the upper Birimian may in fact be rocks of the Tarkwa Group. This idea was not supported by Leube et al. (1990), Hirdes et al. (1992) and Davis et al. (1994) who stated the upper and the lower Birimian are similar in age. Hein et al. (2004) concluded that the Goren Greenstone Belt of north-east Burkina Faso is made up of metamorphosed volcanic and pyroclastic rock units that are intercalated with metasedimentary rocks, thus revising the type section stratigraphy of that belt.

This research focuses on different geological aspects and provides a holistic study of the field area. Due to the lack of field work in the region, basic stratigraphy is not known in many parts of the WAC. However, Tshibubudze and Hein (in review) have established a stratigraphy for the OGGB in a large way. The study area characterizes the greywacke sequence, establishes its internal stratigraphy and looks at its relationships with intrusive rocks that crop out throughout the region. The rocks in the field area are well exposed which is not the case for other parts of the belt, making correlation difficult.

In order to determine the stratigraphy, a detailed sedimentological study was necessary. This was to distinguish between the different sedimentary facies, determine lithologies and a depositional environment in which they formed. The project also considers the structure and metamorphism and the geochemistry of the igneous rocks which play an important role in the interpretation of the tectonic, magmatic and metamorphic conditions.

2.2. Location and Physiography

The study area is situated approximately 2 km east of the town of Markoye and is located 12 km west of the international border of Niger and 38 km south of the border of Mali (Fig. 2). The town of Markoye is located at the divide between the Sahel and the Sahara; everything north of the town is considered to be the Sahara Desert. Thus, the field area is an arid and hot environment with much of the surface covered with sand and loose gravels making outcrop difficult to find in the low-lying areas. The areas of high relief however, are desert mountains that contain a large amount of rock which, unfortunately, was dominated by loose boulders and very little in situ-outcrop.



Figure 1: West African Craton (from Tshibubudze et al., 2009)

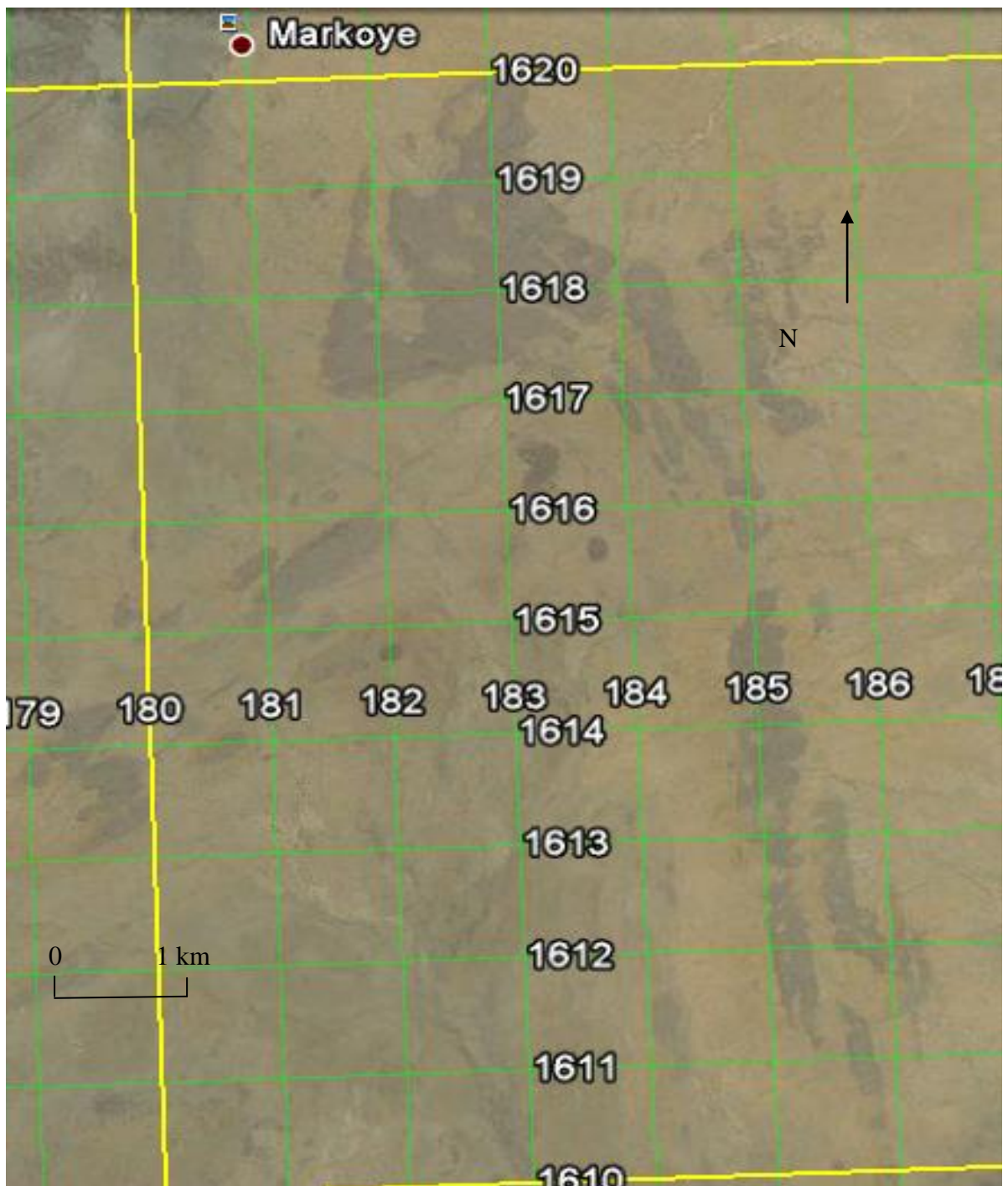


Figure 2: Satellite image of the study area with UTM grid (www.googleearth.com)

2.3. Aims

- To establish a stratigraphic, magmatic and structural column for the study area.
- To interpret a depositional environment.
- To correlate localised structural features with regional tectonic events as described by Tshibubudze et al. (2009).
- To determine whether there is a metamorphic grade change across the field area and understand its relationship with the intrusive material.

2.4. Acronyms, Abbreviations and Standards

Acronyms:

WAC – West African Craton

XRF – X-Ray Fluorescence

ICP-MS – Inductively Coupled Plasma Mass Spectrometry

GPS – Global Positioning System

UTM – Universal Transverse Mercator

PPM – Parts Per Million

REE – Rare Earth Elements

LREE – Light REE

HREE – Heavy REE

LOI – Loss of Ignition

Standards

Chondrite (see appendix)

3.0. Literature Review/Regional Geology

3.1. Stratigraphy

According to Harcöuet et al. (2007) in Hein (2010), the West African Craton (WAC) is made up of Palaeoproterozoic volcanoclastics and metasediments that overlie an inferred granite basement that is Archaean in age. Tshibubudze et al. (2009) and Hirdes et al. (1996) followed Junner's (1935) subdivision to classify the rock formations so that the Birimian sequence is made up of two units; the Lower Birimian and the Upper Birimian. These authors stated that the Lower Birimian consists of dacite, meta-volcanoclastics, greywacke sequences interbedded with siltstone, chert, shale and chemical sediments which have undergone regional metamorphism. The Upper Birimian comprises tholeiitic basalts, granitoid lavas and pyroclastic rocks.

Milesi et al. (1991) and Leube et al. (1990) described the Tarkwa Group as clastic sediments that have undergone regional metamorphism. These authors mentioned that the Tarkwa Group formed as a result of erosion of Birimian rocks and overlies the Birimian Supergroup unconformably. Milesi et al. (1989, 1992) stated that the region to the east of the town of Markoye is made up Tarkwa Group sediments. Tshibubudze et al. (2009) disagreed with these conclusions as the stratigraphy does not match the type section for the Tarkwa Group in Ghana (Milesi et al., 1989, 1991; Bossiere et al., 1996).

Brown et al. (1994) in Tshibubudze et al. (2009) calculated through isotopic studies that there is a major unconformity between the Tarkwa Group sediments and the overlying laterite, which formed during the Cretaceous but was eroded to form glacia in the Eocene-Miocene (Beauvais et al., 2008).

3.2. Sedimentology

The Birimian Supergroup is described by Feybesse et al. (1990), Leube et al. (1990), Hirdes et al. (1996) and Milesi et al. (1991, 1992) and is largely made up of volcanics, chemical sediments and greywacke units with siltstone interbeds. In comparison, the Tarkwa Group

according to Leube et al. (1990) and Milesi et al. (1991) is classified as being predominantly conglomerate units with smaller sandstone and phyllite units.

The formation of thick greywacke sequences generally relates to rapid deposition as to disallow sorting of material. In review of large greywacke units in modern day or recent geological environments, the Wanganui Basin in New Zealand is described by Carter and Naish (1998) and Proust et al. (2005) as a shallow marine environment that is Plio-Pleistocene in age. The basin demonstrates a full range of sedimentary facies. Carter and Naish (1998) identified that equal amounts of sedimentation and subsidence are necessary. Uplift and subsidence were, in the case of the Wanganui Basin, controlled by eustatic changes which created an environment prone to rapid deposition. The Wanganui Basin sits in a back-arc setting at the convergence of the Pacific Plate with the Australian Plate. It is possible that its formation occurred in the same environment. Lithospheric loading and downwarping created by adjacent subduction is credited with basin formation. This resulted in thick units of greywacke being deposited which is similar and therefore significant for the East Markoye region. The tectonic setting of the Wanganui Basin is described in detail by Proust et al. (2005). They explained that the basin is situated on the Australian Plate approximately 200 km behind an active zone of subduction. In this subduction zone, the Pacific Plate is thrust beneath the Australian Plate obliquely. The angle of subduction has remained constant for about 25 million years and is responsible for the creation of large fault systems that lie between the fore-arc basin and the Wanganui Basin. According to Proust et al. (2005) the basin has a depth of 5 km; the sedimentary fill overlies basement rock which consists of a thick unit of greywacke that is Mesozoic in age.

Reviewing literature that describes greywacke formation from the Archaean or Palaeoproterozoic is significant. Similar processes of formation could have occurred owing to the same environment at that point in earth's history. The Pine Creek Inlier of northern Australia contains rocks which are Palaeoproterozoic in age. It consists of metasedimentary rocks and volcanic units that overlie Archaean granite basement (Needham et al., 1988). Needham et al. (1988) stated that the inlier was affected by compressional and extensional tectonism, namely orogeny and rifting respectively. This tectonism was associated with igneous events and post-dated all sedimentation. The basin that makes up the Pine Creek

Inlier was created through processes of extension of the Archaean crust. After rifting took place, sedimentation up to 10 km thick of predominantly clastic and chemical sediments occurred. Needham et al. (op cit.) interpreted sedimentation to have taken place in environments ranging from fluvial to inter-tidal. The Burrell Creek Formation comprises a thick, interbedded sequence of greywacke, siltstone, sandstone and shale that was affected by deformation and diastothermal metamorphism. It is the result of deep water, high energy environment. Needham et al. (1988) stated that these interbedded units make up only a portion of the Bouma Cycle from a turbiditic origin.

3.3. Intrusions

Tshibubudze et al. (2009) studied and described the intrusive bodies in the northern region of Burkina Faso. The Tin Taradat granodiorite tonalite is intruded by the Yacouba Mafic Complex (layered pyroxenite and gabbro suite). The tonalite intruded a granite adamellite west of the Markoye Shear Zone. To the east, it intrudes Palaeoproterozoic sedimentary and volcanic sequences (Tshibubudze and Hein, in review). A swarm of late dolerite dykes which trend WNW and NW cross-cut the supracrustal rocks of the Birimian Supergroup. They are dated at 250 Ma. Tshibubudze et al. (2009) classified dolerite dykes with the same trend in the north-east of Burkina Faso, at Essakane, which also cross-cut supracrustal rocks including greywacke and siltstone. Porphyritic monzonite dykes were identified in the north east part of Burkina Faso and these are the subject of current geochronological studies at the University of Western Australia (Tshibubudze and Hein, in review).

3.4. Regional Tectonics

The tectonism of the West African Craton has been studied in detail by Hirdes et al. (1996), Feybesse et al. (2006), Tshibubudze et al. (2009), Hein (2010) and Tshibubudze and Hein (in review). Hirdes et al. (1996) and Hein et al. (2004) agreed that the Eburnean Orogeny, described by Feybesse et al. (2006) formed as a result of crustal shortening in a SE-NW direction. This was due to the closure of an oceanic basin that was situated between two Archaean cratons. Deformation during the Eburnean Orogeny lead to the creation of shear zones which trend NE-SW. Tshibubudze et al. (2009) described the Markoye Shear Zone and the Takabangou Shear Zone, which trend NNE and are steeply-east dipping. Hein (2010)

stated that there were in fact three phases of deformation; (1) the Tangaeen Event which is characterised by a north-west trending fold-thrust belt (2170-2130 Ma cf., Tshibubudze et al., 2009; Hein, 2010); (2) the polycyclic Eburnean Orogeny which involved continental collision with the orogenic front and associated shear zones in a north-northeast orientation (2130-1980 Ma, Feybesse et al., 2006) and (3) the Wabo-Tampelse Event which is characterised by dextral reverse thrusts and WNW-trending shears and folds (undated cf., Hein et al., 2004; Hein, 2010).

3.5. Metallogenesis

Gold mineralisation in the WAC is classified into five different processes of formation by Milesi et al. (1989) which was reviewed by Beziat et al. (2008) and Hein and Matabane (in review). These classifications are: (1) Mineralisation that occurs in tourmalinised turbidites; (2) Mineralisation of intrusive rocks that occur within disseminated sulphides; (3) Conglomerates which host gold; (4) Lode gold where the gold is formed within arsenopyrite; (5) Lode gold hosted in quartz veins where the gold is in its native state. Milesi et al. (1992) modified their own original classification to just three components as described in Beziat et al. (2008). In this classification, gold mineralisation is described in terms of regional tectonic events where mineralisation is pre-orogenic, syn-orogenic or post-orogenic. According to Beziat et al. (2008), gold in Burkina Faso, in particular is found within or near quartz veins which suggests that the deposits form epigenetically. Tshibubudze et al. (2009) described gold mineralisation at Essakane and observed that it exists in stockwork veins that are made up of quartz and carbonate material. Tshibubudze et al. (2009) explained that Essakane goldfield hosts gold-bearing veins in an anticline that formed in D1 and was dilated in D2.

4.0. Methodology

4.1. Field Methodology

Before going into the field, basic analysis of the study area was completed using satellite images from Google Earth[®] in order to determine the most efficient way of doing fieldwork. Fieldwork was conducted in January 2011. Line and rosette traverses were completed as this was the most effective way of mapping the lithologies, contacts and structural features. It was also the best way of correlating them over the entire the field area. Field mapping was undertaken with a compass clinometer to measure bedding features of the sedimentary units such as dip and strike. A GPS recorded the co-ordinates of the station points (UTM grid system, WGS 84).

Structural mapping was completed; faults were traced out as far as possible, and the orientations and sense of displacement was determined by measuring slickenlines on the fault plane with the compass clinometer. The location of fold axes was established by measuring the dip direction of beds and establishing facing direction using sedimentary features. The station points and geological features recorded in the field were plotted on a satellite image of the study area to allow for progressive visual understanding of the geology as the study continued.

Photographs were taken at most localities. They were necessary and useful when interpreting the geology. Each photograph taken, corresponded to a specific station point and field description. This made the interpretation easier, by simply referring back to a certain point. Selected rock samples were collected for geochemical study, thin section petrography, correct identification of lithologies, and for the building of a comprehensive stratigraphic column. All data, including diagrams, station points, GPS co-ordinates, bedding, structural features and full descriptions of the geology were recorded in a notebook that was used in the write up of the project.

Geological and geomorphologic maps (Fig. 3 and Fig. 5 respectively) were created to depict what geology and physiographic features occur in the field area. A stratigraphic column was also constructed (Fig. 4) from the geological map.

4.2. Laboratory Methodology

Three granodiorite-quartz monzonite samples were submitted for geochemical analysis. This analysis included XRF, which tested for major and trace elements and ICP-MS which tested for trace elements. The analyses were completed at the Earth Lab at the University of the Witwatersrand. The samples were prepared for XRF geochemical analysis which works in the following method:

Summary of XRF Analysis (in house, unpublished).

Major Analysis

All major elements were analyzed for, on an infinitely thick fused disk.

Preparation of the fused disk:

1. All samples were ignited at 1000°C for 40 minutes and the LOI was calculated.
2. The ignited sample was mixed with a commercially available pre-ignited flux (with composition $\text{Li}_2\text{B}_4\text{O}_7 = 47\%$, $\text{Li}_2\text{CO}_3 = 36.7\%$, $\text{La}_2\text{O}_3 = 16\%$) in the ratio of 1:5 and fired for 40 minutes at 1000°C.
3. This was then poured and pressed by a mechanical press into a fused disk.

Data Collection:

All data collection was performed on a PANalytical PW2404 WD XRF with a Rh tube set at 50kV and 50mA an analysis time of 40 sec per an element and 20 sec per a background (backgrounds were measured for Si, Al, Mg, Na and P only). See Table 1 below for specific element data:

Table 1: Major element calibration instrument parameters

Element	Analysis Line	Crystal	Collimator	Detector
Ti	Ka	LiF200	150 µm	Flow
Ca	Ka	LiF200	150 µm	Flow
K	Ka	PE 002-C	550 µm	Flow
Si	Ka	PE 002-C	550 µm	Flow
Al	Ka	PE 002-C	550 µm	Flow
Mg	Ka	PX1	550 µm	Flow
Na	Ka	PX1	550 µm	Flow
P	Ka	Ge 111-C	550 µm	Flow
Ni	Ka	LiF 220	150 µm	Duplex
Fe	Kb	LiF 220	150 µm	Flow
Mn	Ka	LiF 220	150 µm	Duplex
Cr	Ka	LiF 220	150 µm	Duplex

The elemental concentrations were obtained by comparison to 13 known standards. The standards used included: W2, GSP1, BHVO2, AGV2, G2, DTS1, PCC1, BCR2, NIM N, NIM P, NIM S, NIM D, NIM G. A synthetic internal standard was run after every 5 analyses to monitor and compensate for instrumental drift.

Trace Analysis

All trace elements were analyzed for on an infinitely thick pressed pellet.

1. Preparation of the pressed pellet:

Approximately 6g of sample was mixed with three drops of 4% commercially purchased Mowiol (polyvinyl alcohol). This mixture was then pressed under 10 ton pressure into an Al cup using a 40 ton press. The pressed pellet was allowed to dry for 24 hours prior to analysis.

Data Collection:

All data collection was performed on a PANalytical PW2404 WD XRF with a Rh tube set at 50kV and 50mA. The instrument parameters for each element were as per the recommendations outlined by the software Protrace[®].

PANalytical software Protrace[®] was used to process the raw data. The standards used for the calibration were the standards supplied by PANalytical. Protrace[®] drift standards were run after every five analyses to compensate for instrument drift. Internal checks were performed by analyzing known standards as unknowns and comparing them to reported concentrations. The known standards used were AGV2, BHVO2, GSP2, NIM D and NIM S.

4.3. Petrography

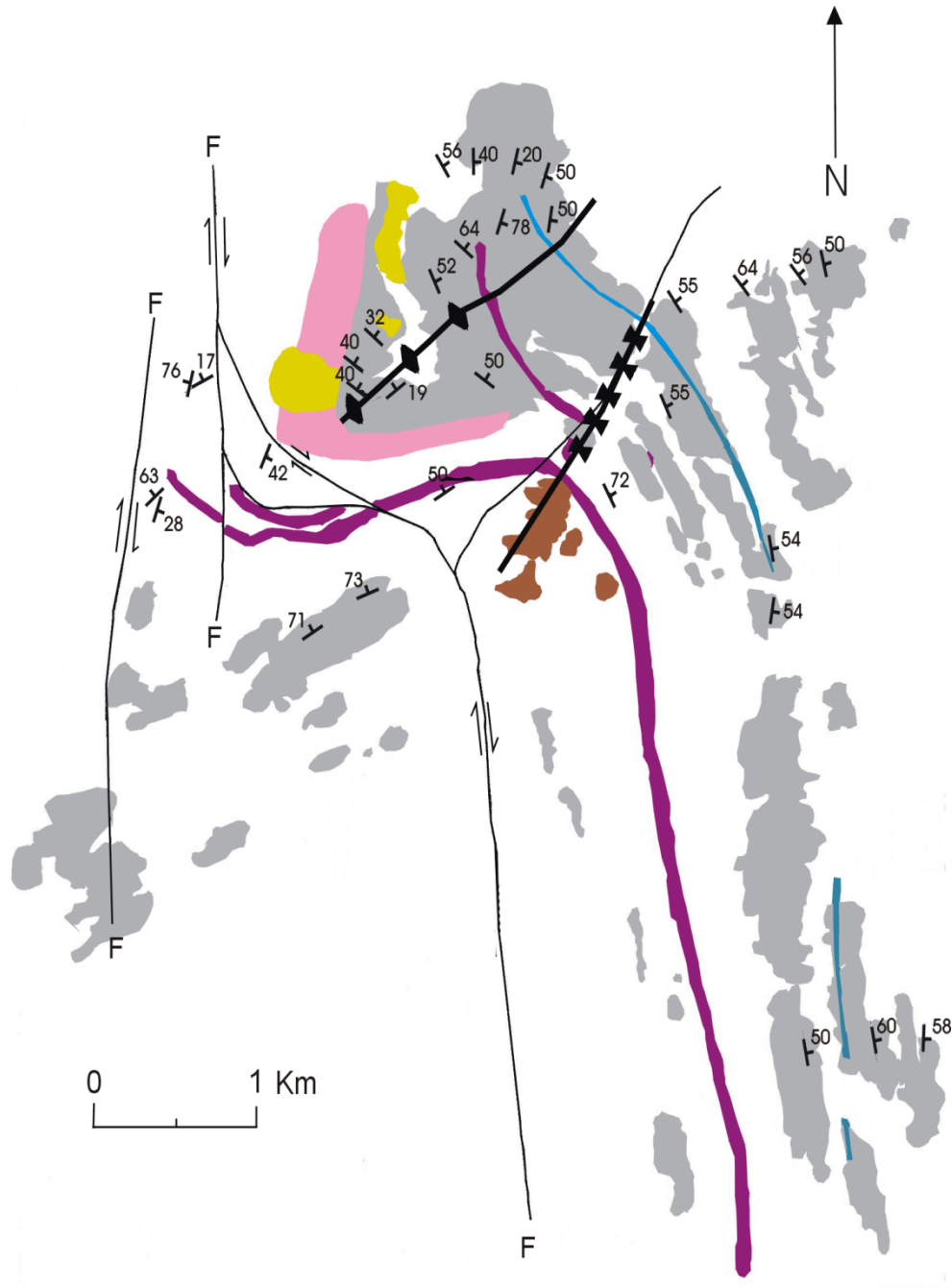
Thin section petrography was completed on the collected samples. Analysis of sedimentary provenance and metamorphic grade was completed. The igneous rocks were also identified and classified. Each thin section was systematically analysed, in particular, when identifying minerals, to ensure consistency and accuracy. Firstly, it was necessary to decide whether the

rock was igneous, metamorphic or sedimentary. For unknown minerals, a mineral identification book was used as well as the following identification tools:

- Relief
- Interference colours
- Pleochroism
- Cleavage
- Twinning.
- Extinction angle
- Interference figure.

Photographs of the thin sections were taken as when necessary. For sedimentary rocks, grain shape, size and modal abundance of clasts and matrix were analysed in order to classify the rocks successfully.

A modal abundance of the minerals was undertaken. For the igneous samples, the Streckeisen diagram (Streckeisen, 1976) was used to identify the rock and for sedimentary samples, the Dott classification (Dott, 1964). Using geochemical data for the igneous rocks, the Streckeisen diagram was created, after the values had been normalised according to the CIPW norm. The two diagrams could then be compared to each other. Le Maitre's classification (Le Maitre, 1989) was also completed using total alkalis versus silica content in weight percent. A spider diagram was created using the XRF trace data and a REE plot using the ICP-MS trace elements.



Legend

- Alluvium
- Palaeosands
- Ferricrete
- Monzodiorite
- Granodiorite-quartz monzodiorite
- Conglomerate
- Greywacke

Figure 3: Geological map of the field area showing structural and bedding data and lithologies.

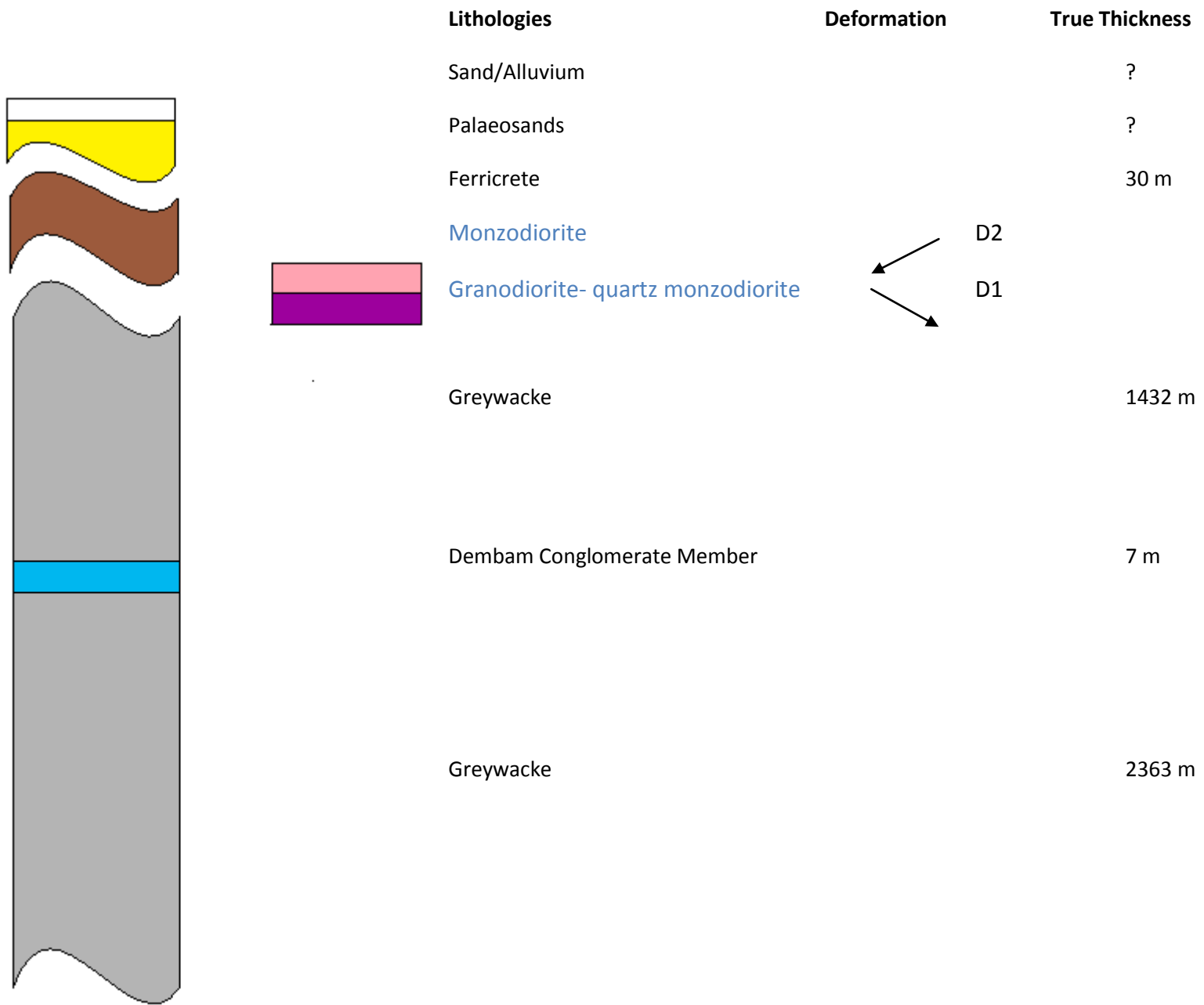


Figure 4: Schematic tecto-stratigraphic column showing lithologies, deformation events and true thicknesses of the units.

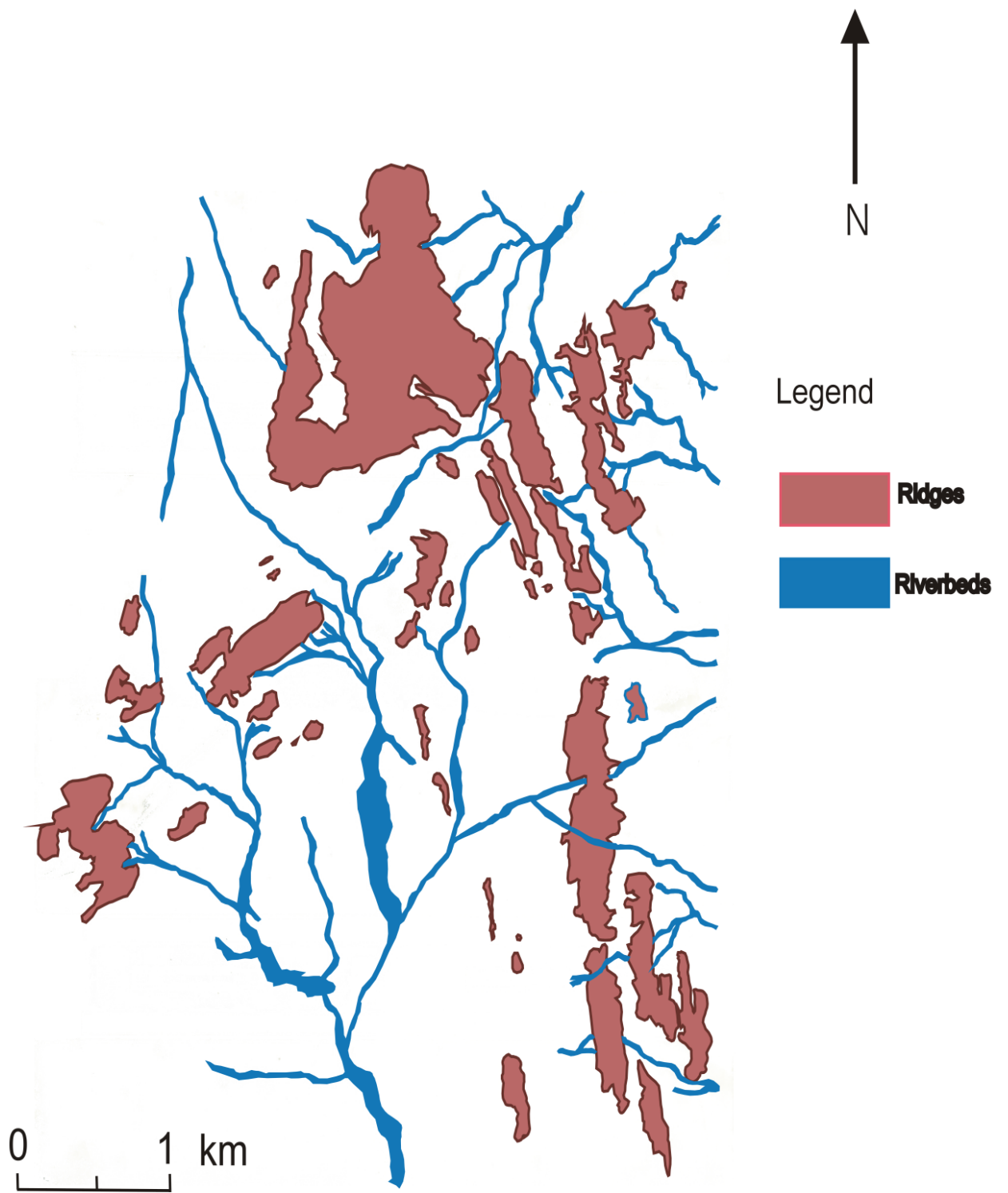


Figure 5: Geographical map representing ridges and river beds (tracks are not included)

5.0. Lithologies

The geology of the study area consists of metamorphosed and folded sedimentary sequences as well as igneous intrusions. The geology is best expressed on ridges to the east and south-east of the town of Markoye. In-situ outcrop is difficult to locate because approximately 95 % of the exposed rock mass is made up of dislodged boulders and blocks (Figs. 6 a & b). This made retrieving accurate measurements difficult. In the low lying areas there is very little outcrop because the rocks are largely covered by sand and colluvium. However, outcrop in the low relief areas tends to be more reliable because it is in-situ. Overall, the entire sedimentary package in the study area is composed of greywacke. This is determined by the abundance of quartz, plagioclase, K-feldspar and accessory minerals such as clinopyroxene. However, some units could be classified as lithic greywackes because they are dominated by lithic fragments and other units as a gritstone-greywacke due to their gritty, coarse texture.

The meta-greywacke is quartz and feldspar-rich, medium-to-coarse-grained, poorly sorted and has exceptionally well preserved sedimentary features in most outcrops. Sedimentary features include cross-bedding, truncated beds, slump folding, scour and fill structures, flame structures and gradational fining upwards sequences. Bedding-facing relationships were used to determine stratigraphic way-up and many of these sedimentary features proved to be good indicators for facing direction. There was a visible amount of variation in terms of composition, grain size, and sorting.

Upward fining sequences are present on a scale, ranging from 3-15 centimetres per cycle of deposition. The cycles are often truncated (a scour base), by the next one. Cross-bedding is seen at almost all outcrops and varies in scale from centimetres to metre scale. The cross-bedded greywacke exhibits differential flow direction. All depict younging direction towards the east when not near a fold hinge. Truncated beds, upward-fining sequences, scour and fill and less commonly, flame structures aided in understanding and determining facing direction. Fine, thinly laminated mud drapes were intercalated with the greywacke throughout the sequence. Thin chert beds exist but were often broken up and suspended in the overlying sedimentary rocks as rip-up clasts (intraclasts). The greywackes are deposited as turbidites and have consistent fining upwards sequences. This suggests that each unit is deposited under

the influence of gravity and makes up part of the Bouma Cycle (Bouma, 1962). In the field area, the bottom layers of the cycle was seen; (1) massive and graded; (2) plane parallel laminae and (3) ripples, wavy or convoluted laminae (Bouma, 1962; Shanmugam, 1997).

There is a variable amount of orthoclase in most samples, (modal abundance ranging from 2-15%) as shown by very prominent Carlsbad twinning and the typical smoky grey to white colourations. Granophyric texture in some clasts provided evidence of simultaneous rapid growth of quartz and alkali feldspars in the source rock region (Barker, 1970). Perthitic textures were also evident in some clasts indicating that the clast source region underwent exsolution between plagioclase and K-feldspars (Nesse, 2000). Clinopyroxene was present in most of the samples in a relatively high abundance of 5-10%. They are 0.2 to 1.5 millimetres in length, subhedral, are twinned and occasionally exhibit alteration rims.

Epidote and chlorite are present in all the samples and indicate metamorphism to greenschist facies. Hornblende exists in some of the greywackes, although in low proportions, and is interpreted to be detrital grains derived from the source rock region. The greywacke units have undergone ferruginization in localised areas. This is noticeable due to iron staining, which is prominent throughout the rock. Muscovite appears as an alteration mineral in low proportions, less than 2 %.

A matrix-supported, polymict conglomerate member (hereafter termed the Dembam Conglomerate Member), with a thickness of ten metres, is interbedded within the greywacke. It crops out in the north of the field area as a cobble conglomerate. The unit strikes north-south and thins out towards the south. The cobbles are sub-angular to sub-rounded and cemented in a cross-bedded matrix of poorly sorted and coarse-grained greywacke. There is a variety of cobbles making up this conglomerate such as fuchsitic chert, black chert, granite (*sensu-stricto*) basalt, andesite, finely laminated sandstone interbedded with mudstones that host small-scale slump folds, quartz vein, and quartz-rich meta-sediments. The conglomerate is similar to that described by Tshibubudze and Hein (in review) and is the focus of current geochronology studies at the University of Western Australia.

Table 2: Rock type, bedding data and location of station points.

Station point	GPS Coordinates		Rock name	Strike	Dip	Dip direction	Facing
2	181875	1618862	metagreywacke	007	82	e	e
5	182766	1618875	metagreywacke	012	78	e	e
7	182985	1618898	metagreywacke (with granite clasts)	002	44	e	e
8	183152	1618883	metagreywacke	006	50	e	
9	183183	1618869	metagreywacke	002	48	e	
11	182983	1618872	metagreywacke	004	66	e	
18	181605	1617565	metagreywacke	312	40	e	e
19	181740	1617843	metagreywacke	322	32	e	
23	182235	1618362	metagreywacke	340	52	e	e
24	182468	1618641	metagreywacke	320	62	e	e
28	182643	1617405	metagreywacke	315	60	e	e
29	182614	1617399	metagreywacke	322	50	e	
36	183637	1616279	metagreywacke	338	72	e	e
41	184087	1617122	metagreywacke	340	50	e	e
42	184301	1617219	metagreywacke	328	40	e	
43	184315	1617356	metagreywacke	329	50	e	e
47	184986	1614898	metagreywacke	010	60	e	e
48	184916	1615599	metagreywacke	351	56	e	e
49	184979	1615755	conglomerate	355	58	e	
50	184879	1615803	metagreywacke	340	54	e	e
51	185047	1613868	metagreywacke	352	56	e	e
52	185004	1612997	metagreywacke	355	54	e	e
53	185058	1613003	conglomerate	354	62	e	e
54	185518	1612499	metagreywacke	351	54	e	e
55	185565	1612466	metagreywacke	358	60	e	e

56	186193	1612061	metagreywacke	003	58	e	e
57	186021	1612078	metagreywacke	348	52	e	e
58	185854	1612076	metagreywacke	350	60	e	e
59	185790	1612076	metagreywacke	352	72	e	e
60	185671	1612030	metagreywacke	352	65	e	e
61	185236	1612027	metagreywacke and conglomerate	352	50	e	
62	185611	1611322	metagreywacke	336	62	e	e
63	184142	1613115	metagreywacke	352	60	e	e
64	182292	1619442	metagreywacke	334	56	e	e
65	182551	1619462	metagreywacke	001	40	e	e
74	183138	1619334	metagreywacke	012	50	e	e
75	182074	1619616	metagreywacke	005	45	e	e
76	184155	1618089	metagreywacke	342	55	e	e
77	184693	1618206	metagreywacke	327	64	e	e
78	185044	1618260	metagreywacke	331	62	e	e
79	185213	1618382	metagreywacke	323	56	e	e
80	185352	1618389	metagreywacke	351	50	e	e
81	185391	1617737	metagreywacke	342	56	e	e
82	185215	1617765	metagreywacke	350	60	e	
83	185059	1617617	metagreywacke	344	58	e	e
95	181146	1616222	metagreywacke	360	80	e	w
100	181584	1615817	metagreywacke	062	71	nw	nw
101	180977	1615638	metagreywacke	034	67	nw	nw
102	180875	1615545	metagreywacke	049	64	nw	nw
103	181078	1615458	metagreywacke (granite clasts)	044	50	nw	nw
104	182303	1616301	metagreywacke	062	44	nw	nw

105	182390	1616420	metagreywacke	058	50	nw	nw
108	180176	1616753	metagreywacke	039	61	se	
110	120284	1617000	metagreywacke	348	41	e	e
111	180258	1617481	lithic metagreywacke	013	76	w	w
112	180330	1617461	lithic gritstone-greywacke	053	17	w	w
116	179992	1616297	metagreywacke (with grad. lithic beds)	018	28	e	
119	179985	1616409	metagreywacke with lithic grad. Beds	035	50	w	
120	181978	1616193	metagreywacke	038	63	nw	nw
121	182008	1616133	metagreywacke	039	68	nw	nw
122	182080	1616141	metagreywacke	070	64	n	n
123	182151	1616292	metagreywacke	274	74	n	
124	182261	1616286	metagreywacke	042	60	nw	
125	182311	1616339	metagreywacke	097	56	n	n
126	182439	1616434	metagreywacke	070	58	n	n
127	182516	1616458	metagreywacke	072	54	n	n
128	182871	1616456	metagreywacke	110	57	n	n
130	183015	1616511	metagreywacke	098	68	n	n
134	183461	1617196	gritstone with lithic fragments	149	56	e	e
139	183147	1617314	metagreywacke	040	64	se	se
172	181923	1617334	metagreywacke	047	19	n	n
173	181774	1617276	metagreywacke	065	50	n	n
174	181660	1617315	metagreywacke	114	40	n	n
175	182924	1617409	metagreywacke	006	52	e	e
176	182873	1617417	metagreywacke	089	18	n	n
189	182896	1617422	metagreywacke	074	39	n	n
190	182880	1617415	metagreywacke	038	46	n	n
191	182865	1617412	metagreywacke	024	22	n	n

192	182815	1617413	metagreywacke	143	72	w	w
193	182798	1617440	metagreywacke	073	32	n	n
194	182781	1617412	metagreywacke	162	56	e	e
195	182741	1617425	metagreywacke	045	38	n	n
196	182722	1617391	metagreywacke	172	56	e	e
206	184892	1611275	Metagreywacke	163	60	e	e
207	185143	1611301	greywacke with lithic fragments	163	58	e	e

Laterite-capped ridges occur in isolated locations in the OGGB. It is reddish-brown in colour, coarse-grained and porous. It formed during the Cretaceous period (Brown et al., 1994; Burke and Gunnell, 2008) and was subsequently eroded during the Eocene-Miocene epochs (Brown et al., 1994; Beauvais et al., 2008). These laterite-capped ridges mark a hiatus in the stratigraphic record since the underlying sediments are Palaeoproterozoic in age.

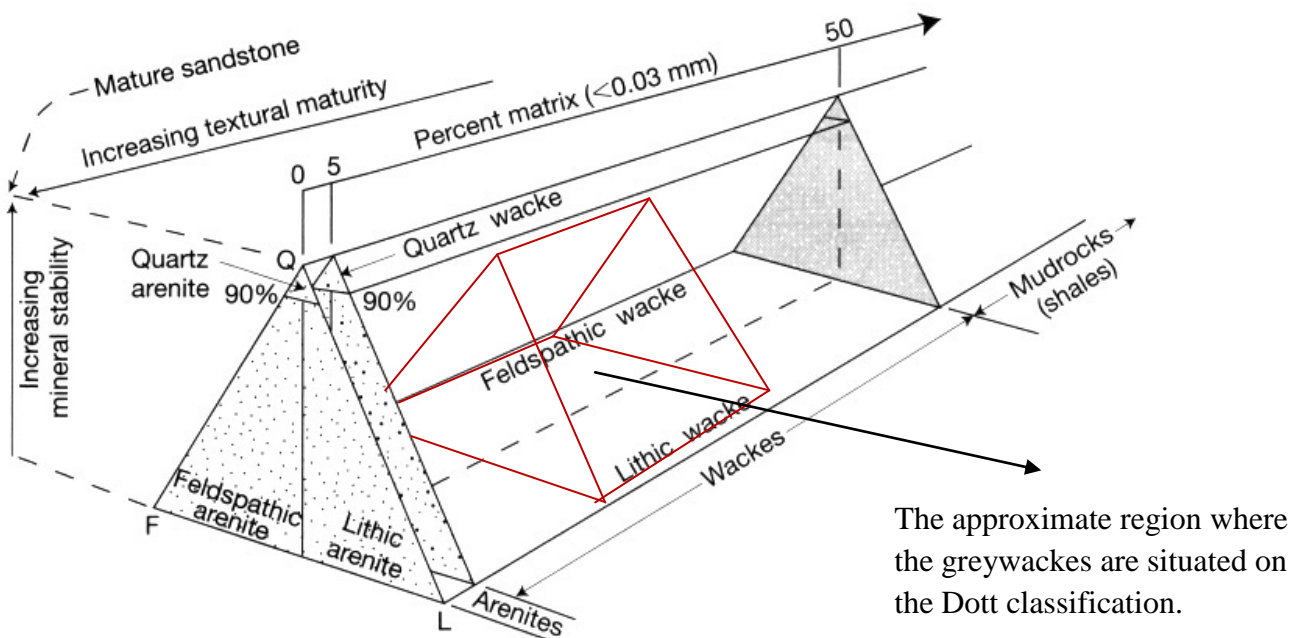


Figure 7: Dott Classification Scheme for sedimentary rocks showing that greywackes contain 15-50% matrix (Dott, 1964).

Samples of intrusive rocks in the field area and other parts of the greenstone belt were geochemically analysed by Tshibubudze and Hein (submitted). They are classified according to Streckeisen (Streckeisen, 1976) as monzodiorite to quartz monzodiorites. These dykes crosscut the field area and trend east-west. They were folded. They have a width ranging between 30-50 metres. They consist of large, euhedral plagioclase crystals, up to 2 centimetres in size, within a groundmass of hornblende, quartz and clinopyroxene. The dykes are dark coloured, medium-grained rocks that have a porphyritic texture. They have undergone metamorphism to the middle greenschist facies as shown by the presence chlorite and epidote. The chlorite is commonly seen replacing large plagioclase crystals.

Euhedral, deuterically altered plagioclase phenocrysts exhibit remnant albite twinning. Clinopyroxene occurs in variable amounts but usually between 15 and 30 % modal abundance. The clinopyroxene shows alteration rimming, twinning and less commonly exsolution lamellae. There are smaller (0.1-0.3 mm), subhedral to anhedral, unaltered plagioclase crystals with albite twinning and small, interstitial quartz that comprises the intercumulus minerals.

A granodiorite to quartz monzodiorite dyke also crosscuts the study area. It is approximately 50 m wide and consists of large plagioclase crystals, both rounded and subhedral to euhedral in shape. There is a 10-20 %, visible proportion of alkali feldspar and quartz. In hand sample, hornblende and clinopyroxene are visible. An east-west profile was conducted across the intrusion to establish if the dyke was originally a sill. No significant change in crystal size or composition was observed. A partially bleached contact is seen in a river bed. Hornfels is situated proximal to the dyke. Micro-veins or brecciation is visible which appears to be a chill margin. However, it occurs only on the dyke and not within the hornfels. At the contact, plagioclase phenocrysts are not as large and are more commonly euhedral rather than rounded. In thin section, it shows an altered, lower-middle-greenschist metamorphosed rock. It has an abundance of interstitial quartz, mostly less than 20 % plagioclase and long bladed crystals of hornblende. Some occurrences have secondary, unaltered, smaller, anhedral plagioclase. It has a porphyritic texture shown by a fine-grained groundmass that surrounds large plagioclase phenocrysts. There are quartz inclusions within the altered plagioclase. This plagioclase exhibits relic albite twinning. Clinopyroxene makes up approximately 10 % of

the rock and is rimmed by hornblende. Chlorite replaces hornblende. There is a high quartz concentration (~85-90 %) in a number of the granodiorite samples, which can be interpreted as crustal contamination or wall-rock interaction during emplacement.

The dykes crop out throughout the OGGB and host gold mineralisation just north of the Essakane goldfield (Tshibubudze and Hein, in review). They are deuterically altered indicating low temperature metasomatism related to primary mineral changes in the magma before solidification. The crystals remain the same in composition but are essentially destroyed as the mineral begins to break down compositionally (Neuerburg, 1958). This type of alteration is common and can affect mafic to felsic rocks during crystallisation. An example where deuteric alteration affects quartz monzonites, similar in composition to the dykes of the field area, is from the Boulder Batholith in Montana, USA. In this case, the alteration is related to the formation of ore deposits hosted within the intrusion (Neuerburg, 1958).

6.0. Structure and Metamorphism:

The field area has been metamorphosed to lower- middle greenschist facies as shown by the ubiquitous presence of chlorite and epidote. There is no apparent fabric in the samples. Metamorphic derived micas and amphiboles are lacking. A fabric at such low grade with fine-grained minerals (epidote and chlorite) would develop only a vague mineral alignment, if any (Prof. Cawthorn, pers. comms.). In thin section, a slight fabric is visible, where minerals are aligned but this occurs adjacent to quartz-filled fractures and not as a result of metamorphism. The sediments that are situated approximately 20 metres or less away from dykes have undergone contact metamorphism to hornblende-hornfels facies, where no internal structure or primary bedding can be seen (i.e., grains and sedimentary features) (Fig 8). The hornfels is fine grained (less than 0.1 mm). However, more often than not, these rocks express their sedimentary character as compositional variation, as seen on weathered surfaces. The rocks are silicified and glassy.

The field area and the OGGB do not exhibit the correct criteria for large-scale contact metamorphism. One would expect to see a prominent zonation to an igneous mass. In the case of the Pine Creek Inlier, a zonation from hornfels to greenschist is mappable, with a definable biotite isograd (Hein, 2003). Burial metamorphism is an active process which would have involved basin subsidence and a resulting increase in the geothermal gradient. There would be an increase in pressure and temperature as well as the development of bedding parallel cleavage at depth (Vernon and Clarke, 2008). Cleavage is not present in the rocks, even at a petrographic scale and there is no mineral fabric suggesting burial metamorphism. Diastathermal metamorphism better explains the process of metamorphism for the rocks in the OGGB.

With respect to the greywacke, hornblende occurs in minor proportions. The hornblende does not exhibit any foliation, which suggests it was derived from an igneous source that was deposited as detrital grains. The metamorphism in the field area correlates with Tshibubudze et al. (2009) and Tshibubudze and Hein (in review) who concluded greenschist metamorphism is dominant throughout the OGGB. The metamorphic grade of most of the greenstone belts of the Birimian Supergroup have been described as greenschist facies

(Bossiere et al., 1996; Hirdes et al., 1996; Beziat et al., 2000). On a cratonic scale, the Eburnean Orogeny and the emplacement of numerous large, calc-alkaline plutons is suggested to be responsible for a regional, low-grade metamorphic terrane (Bossiere et al., 1996; Hirdes et al., 1996; Beziat et al., 2000). There is no evidence to suggest that contact metamorphism occurred on such a large scale that would give rise to these greenschist-facies rocks within the field area. The rocks of the OGGB were subjected to greenschist facies conditions with the exception of a few localities where amphibolite and granulite facies was attained, adjacent to plutons (Tshibubudze et al., 2009).

With respect to structure, the gold deposits in the OGGB are structurally constrained within shear zones and their associated splays (Tshibubudze et al., 2009; Tshibubudze and Hein., in review). The entire sequence of greywacke was folded and re-folded during two deformation events. Field data collected on bedding-facing relationships shows that around the fold hinges the beds dip and face in opposite directions, compared to the rest of the region where everything faces and dips toward the east. There are small scale m-folds where beds dip and face in alternating directions over 5 to 10 metre intervals. The axial plane of a macroscopic thrust fold trends NNE.

There is a N-S trending fault system that traverses the field area with minor subtending splay faults, hereafter termed the Ludovic Fault System. Field measurements of down dip slickenlines, accretion steps on the fault plane and large scale S-C fabrics indicate that the faults were displaced. Dextral-normal displacement occurred with the western block up relative to the downward moving eastern block. There is a large quantity of quartz, with saw-tooth crystal growth (open-spaced fill). The quartz is often dark in colour due to high stress, and was found around the areas of faulting which allows for relatively simple mapping of the fault plane. Bleached greywacke is also found in abundance around the fault plane. This suggests that fluid had moved through the rock mass. The main fault, which trends from north-south, has an anticlockwise flexure, which was validated by measuring strike changes of the greywacke along its length. East-west and north-south trending fractures and joints are common in the area. The presence of open space quartz, a S-C fabric, down dip slickenlines and accretion steps indicate that the Ludovic Fault System is an extensional fault.

An equal area stereographic projection (Fig. 9) of the poles to planes of the bedding data represents two broad clusters which straddle a calculated girdle of $111^{\circ}53'S$. The spread of polar data about the primitive circle is the result of folding in D1 and D2 (c.f., Tshibubudze et al., 2009; Tshibubudze and Hein, in review). The outlier poles are interpreted as being affected by drag folding against local faults which changed the polar orientations dramatically.

The stereographic projection of poles to bedding correlates well with data provided by Tshibubudze et al. (2009) who concluded the rocks of the OGGB were deformed and folded by two deformation events i.e. the Tangaeen Event and the Eburnean Orogeny. To determine the mean fold axis, the data was split into the different fold limbs.

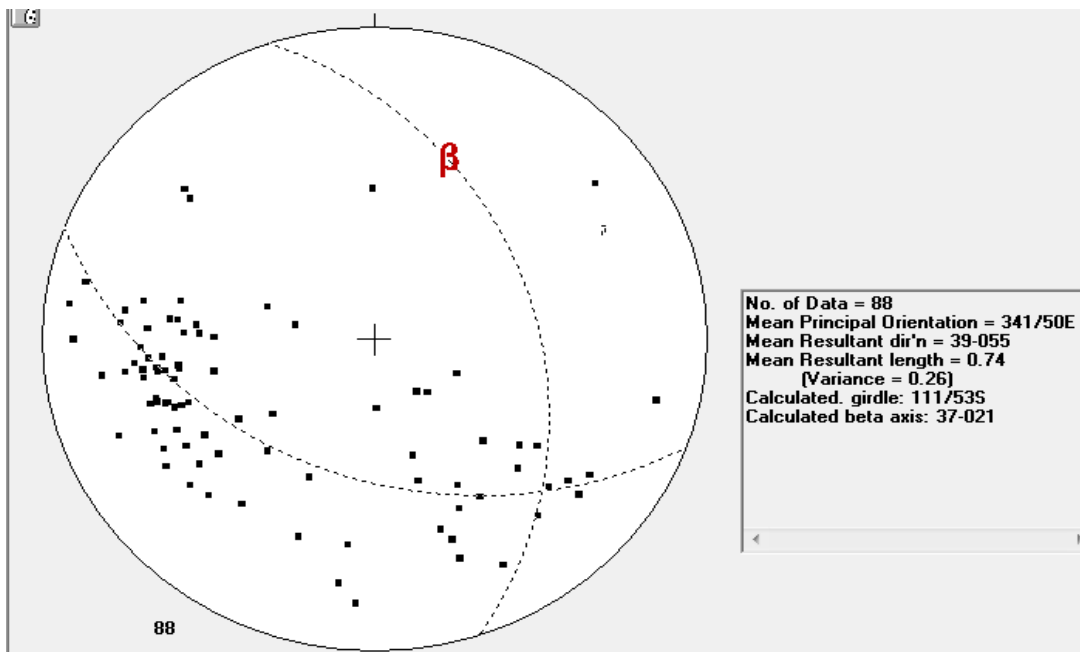


Figure 9: Stereographic projection of poles of the bedding data.

7.0. Geochemistry of Igneous Rocks

Normalising the major elements to the CIPW norm and calculating the percentages of quartz, plagioclase and orthoclase for the samples, gave results of granodiorite to quartz monzodiorite on the Streckeisen diagram (see Fig. 10a). For the rocks termed monzodiorite to quartz monzodiorite, geochemical results from Tshibubudze and Hein (submitted) were used. All these results place these rocks within a calc-alkaline field according to Streckeisen (1976). Figure 10b shows the major elements plotted on the same graph, but instead of using the CIPW norm, modal abundances from thin section analysis were determined. There is a slight variation between the two sets of results which can be explained by the fact that the CIPW norm is a theoretical estimate that has a higher margin of error. This is why it is necessary to compare those results with modal abundances. Overall, the samples are calc-alkaline in composition, which indicates a good correlation between the data.

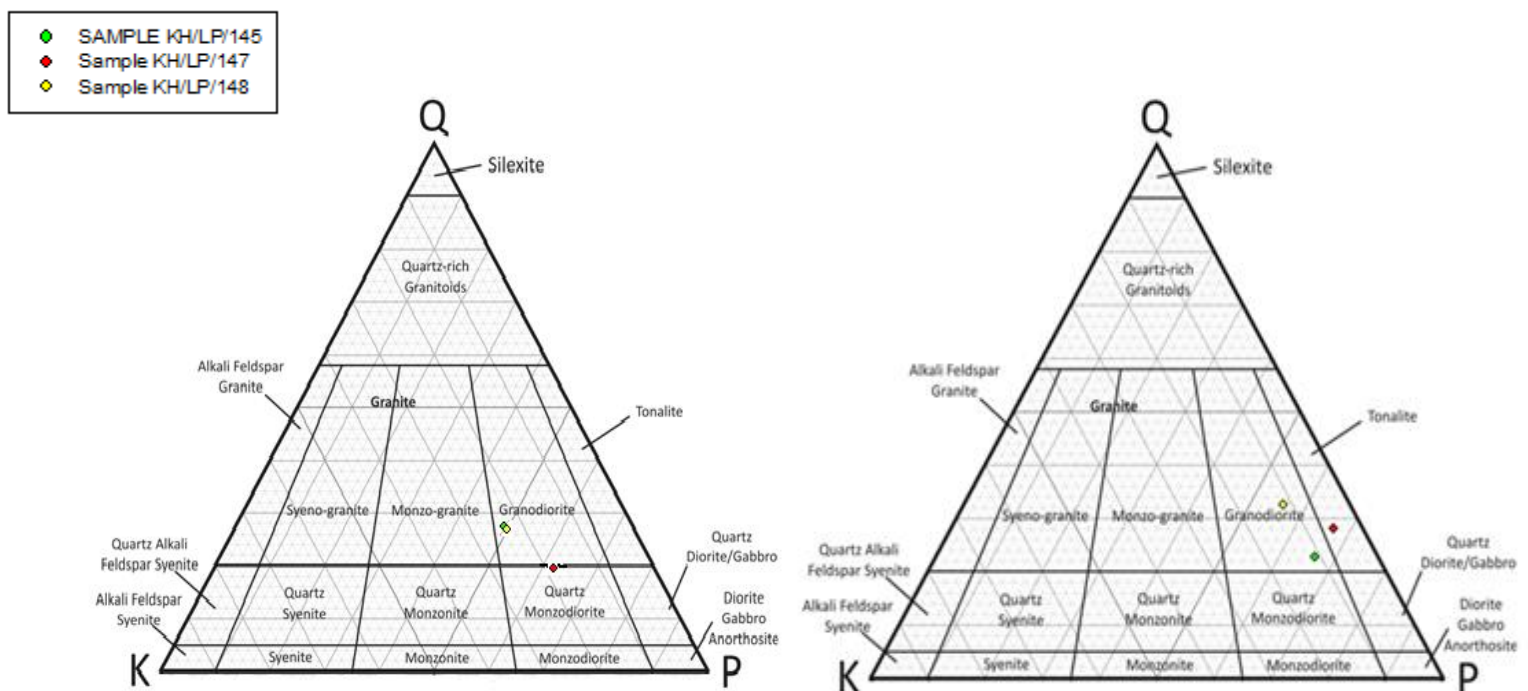


Figure 10 a & b: Classification of samples KH/LP/145, KH/LP/147 and KH/LP/148 on a Streckeisen Diagram after Streckeisen (1976) using the CIPW norm and modal abundance.

Plotting total alkalis against silica content (see Fig. 11) yielded slightly different results but essentially the samples still fall within the granodiorite field of the Le Maitre (1989) classification system. Sample KH/LP/145 and KH/LP/147 are very similar in composition on both classification diagrams; however they are more granitic in composition according to the total alkalis versus silica. Whereas sample KH/LP/148 on the Streckeisen diagram is situated on the field boundary between a granodiorite and a quartz- monzodiorite and on Le Maitre's classification it is well within the granodiorite field.

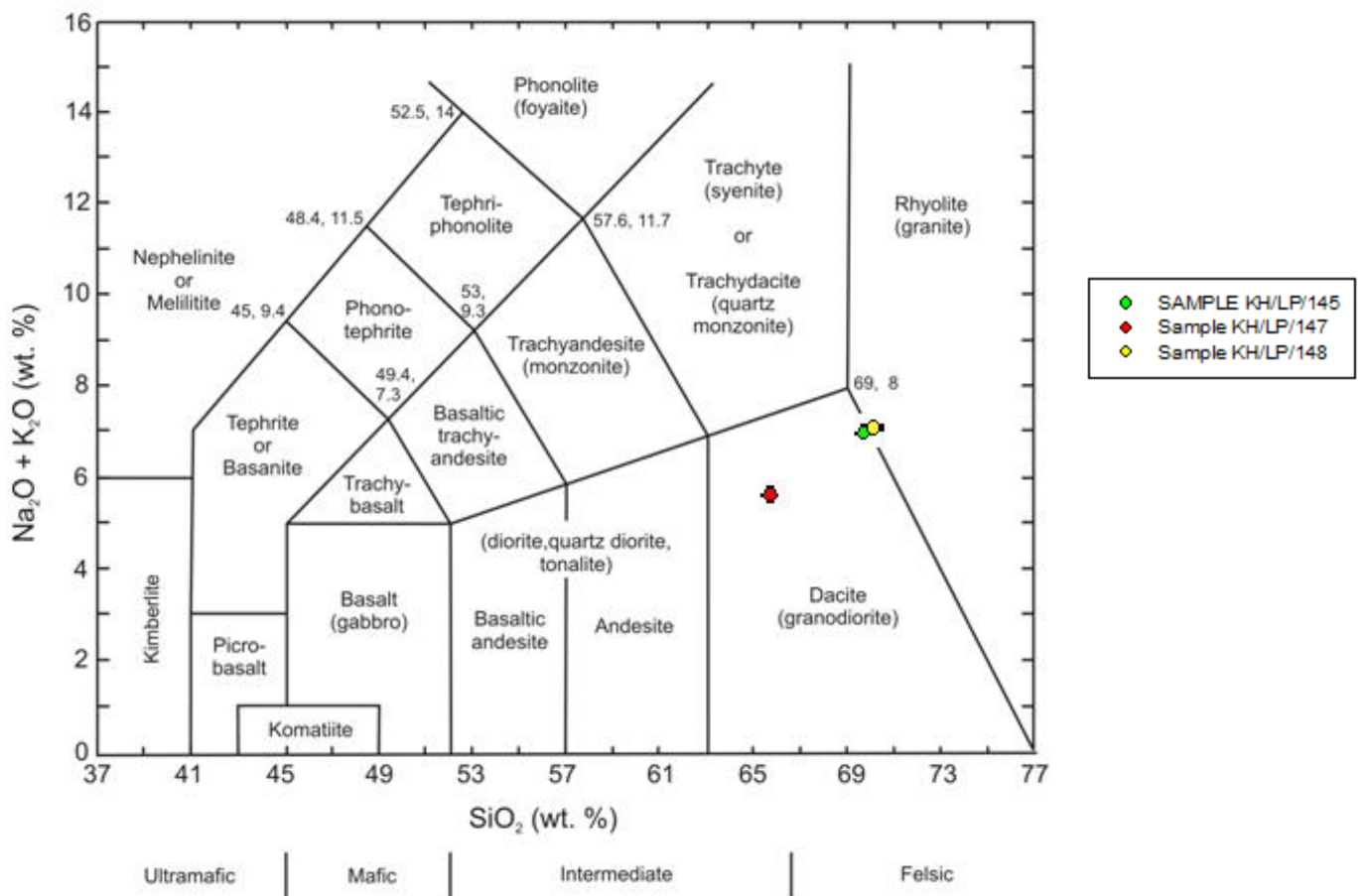


Figure 11: Total alkalis versus Silica Diagram after Le Maitre (1989).

The trace element data of the granodiorite to quartz monzodiorite is represented as a spider plot (see Fig. 12), with the sample composition values in ppm normalised to chondrite. The elements are ordered on the x-axis in increasing incompatibility. There is a large negative anomaly for nickel in all three samples. The plots are almost identical which shows good

correlation and consistency within the dyke. There is an initial decrease from Sc but it rises again after Ni and the overall trend is an increase in the order from more compatible to more incompatible.

Spider Diagram of Trace Element Data

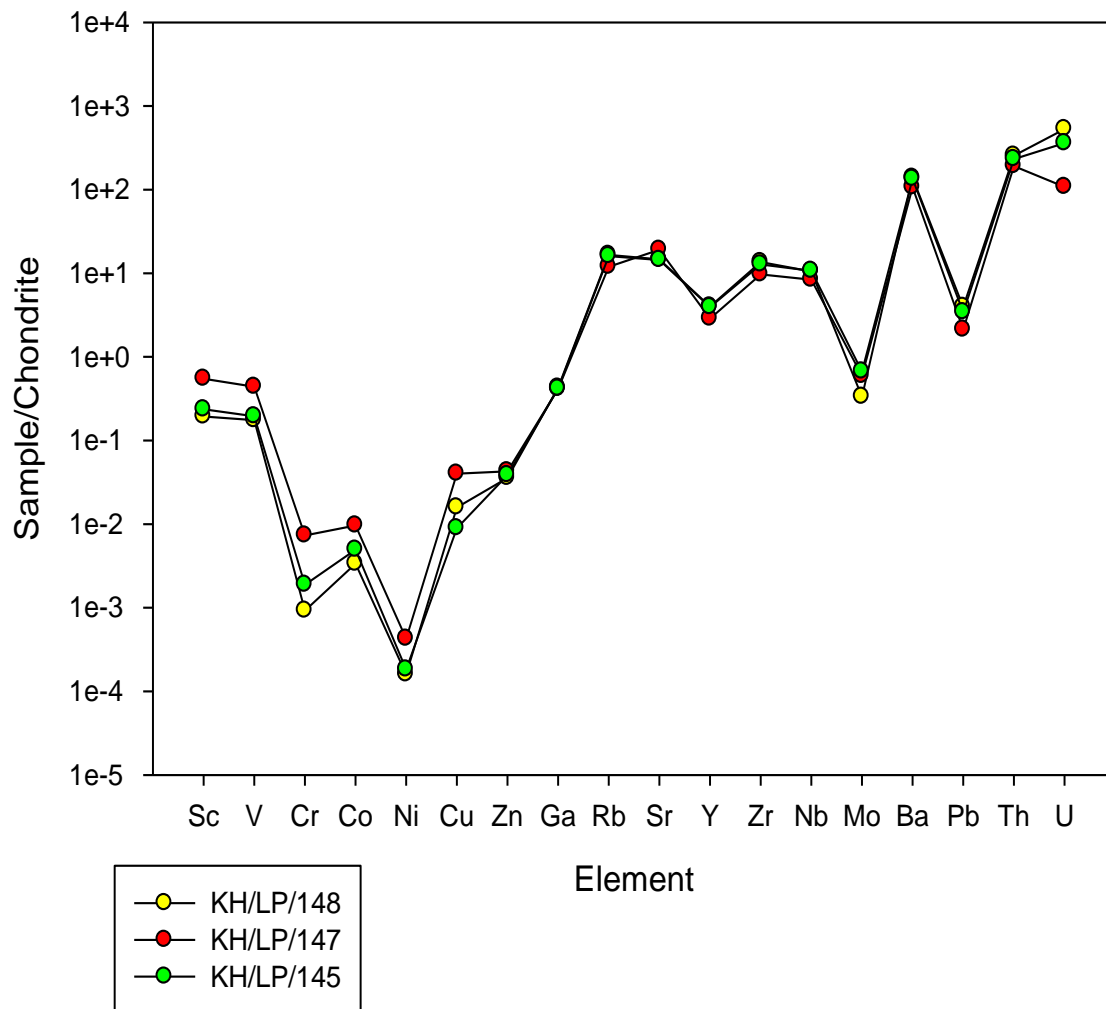


Figure 12: Graph showing trace element concentration in order of increasing incompatibility (left to right).

These data are normalised against chondrite meteorites, as its average composition represents the best approximation for a complete solar abundance. The graph (Fig. 13) is plotted on a semi-log scale to show the exponential variation between LREE and HREE relative to chondrite. The REE plot overall shows a decrease of one order of magnitude from LREE to HREE. From La to Eu there is a steep decline in concentration from which point the HREE start to level out and remain fairly constant. Both the LREE and the HREE are enriched relative to chondrite, which is constant on the line $y=1$. However, relative to each other, the LREE are more enriched. Small, negative Eu anomalies are visible for sample KH/LP/ 145 and KH/LP/148, but are not very significant due to their size. It is possible that because there is a slight enrichment in Gd in these rocks, that Eu appears to be anomalously lower relative to Gd.

REE plot for the quartz-monzodiorite samples

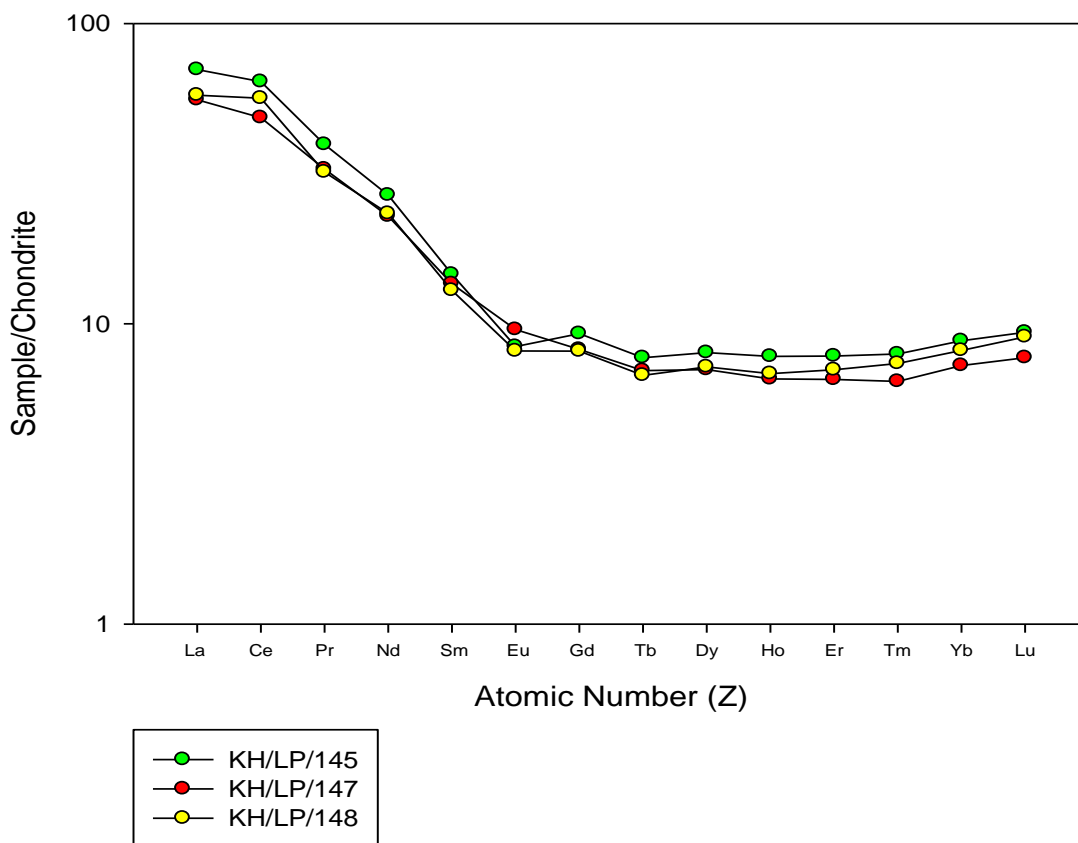


Figure 13: Graph depicting the REE concentrations in the quartz-monzodiorites.

The geochemical and thin section analyses provide a classification of the intrusive rocks. Even though there is a slight variation between the two Streckeisen ternary plots and Le

Maitre's total alkali versus silica graph, all the samples result in being calc-alkaline in composition. This falls within the tonalite-trondjemite-granodiorite (TTG) suite that characterizes most of the Palaeoproterozoic plutonic bodies of the WAC.

These rocks are intermediate intrusives and therefore have a higher concentration of incompatible elements compared to a mafic composition, because these incompatibles preferentially partition into the liquid phase until they are forced to crystallise. True granites will have higher concentration of incompatible elements. The anomalous nickel concentration in the spider plot is a result of its compatibility with the mineral olivine. By the time enough differentiation and fractionation due to partial melting occurs to produce intermediate-felsic compositions, Ni has already been used up in the production of mafic rocks. Cr also preferentially partitions into orthopyroxene crystals when mafic-ultramafic magmas are crystallising and therefore has a negative anomaly in these samples.

The REE data normalised to chondrite shows a magma that had an overall enrichment relative to chondrite. It also had a larger enrichment in LREE relative to HREE. This is indicative of intermediate-felsic rocks as all the incompatible elements are retained in the melt until they are forced to crystallise. A number of partial melting cycles will have occurred before this magma formed as it does not represent ultramafic-mafic magmas but rather magmas that make up continental crustal material. Small Eu anomalies occur in the REE plot. This indicates that Eu most likely replaced Ca in the plagioclase crystal structure during the last phase of crystallisation.

8.0. Depositional Environment

There are two major stratigraphic sequences in this region of the OGGB; a thick lithic-feldspathic greywacke and an interbed of conglomerate. These are unconformably overlain by ferricrete. The unconformity marks a significant hiatus. Sedimentary features in the greywacke including cross-bedding, gradational bedding, scour and fill structures, ripple marks, upward fining sequences, slump folding and mud drapes indicate a palaeo-environment that was turbiditic in character (Fischer and Schmincke, 1994; Boggs, 2006). Slump structures are interpreted to form as result of gravity sliding in a shallow marine environment with a slurry of mud that has been deformed within the greywacke (Ravanas and Furnes, 1995). They are not on a large scale like melange deposits but are known from subduction type settings, when on shallow to steep marine slopes that allow for gravity failure (Ravanas and Furnes, 1995). Chert layers are interlaminated within the greywackes and have been altered to fuchsitic chert. They commonly form rip-up clasts within close proximity of the chert bed indicating primary chert. This is interpreted as possible seasonal changes or time periods where erosion and deposition were not rapid and allowed for the deposition of chert.

Turbidite currents account for the rapid deposition of a large volume of sediment. The sediment is poorly sorted and has angular to intermediate grain shapes. It also contains lithic fragments and igneous-derived minerals such as clinopyroxene. Clinopyroxene is not as resistant to weathering as minerals such as quartz and plagioclase and will therefore decompose rapidly with increasing distance from the source (Albarede, 2003). Its presence in the metasedimentary rocks of the field area thus indicates that deposition in the sedimentary basin was proximal to the source. The turbidite is interpreted as being formed in a shallow marine or shelf environment. It is associated with deltaic systems, which are common depositional environments in arc basins (Fischer and Schmincke, 1994). The sedimentary features in the greywacke also assist with the depositional environment. Slump folding is indicative of deltaic and turbiditic deposition due to its instability caused by swift deposition on a steep slope (Boggs, 2004). Scour and fill structures occur in deltaic environments, especially delta fronts (Boggs, 2004). The fining upwards sequences, within each deposition cycle represents small scale Bouma sequences (Fig. 17) that are indicative of turbidite flows (Bouma, 1962). In the study area, Bouma T_a, T_b and T_c are commonly seen in the greywacke

sequence with occasional mud drapes making up the Bouma $T_{e/f}$ layer of the sequence. Layers A and B often occur together in coarser grained sediments which is the case for the greywackes (Boggs, 2004) as shown by Figure 14.

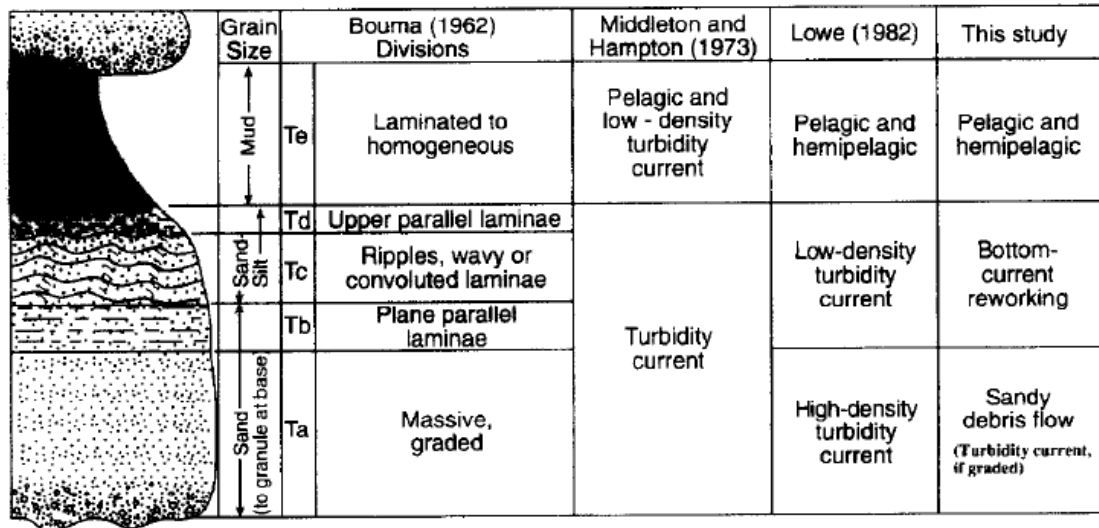


Figure 14: Classic model of the Bouma Cycle (Shanmugam, 1997).

Stratigraphically, the entire field area was previously assigned to the metasedimentary rocks of the Tarkwa Group (Milesi et al., 1989, 1992; Castaing et al., 2003) which represents the erosional product of the Birimian Supergroup. The correlation with the Tarkwa Group was based on the single conglomerate unit in the study area and several conglomerate bands near the Essakane gold mine (Milesi et al., 1989, 1991; Bossiere et al., 1996). The Tarkwaian conglomerates in the type section in Ghana consist mostly of quartz vein clasts and a minor proportion of quartzite pebbles in a dark, fine-grained, sandy matrix. However, the conglomerate found in the study area have similarities to those described by Tshibubudze et al. (2009) and Tshibubudze and Hein (2011) and host clasts of fuchsitic chert, black chert, quartz, dacite, granodiorite and meta-sediment. These clasts are set in an immature greywacke matrix with lithic fragments, gradational bedding and cross-bedding.

Further argument for the rocks in the field area not to be considered Tarkwa Group sediments is that there is no visible regional unconformity that marks the base of the overlying Tarkwa sediments. A continuous stratigraphy is seen throughout the entire OGGB with no unconformity (Tshibubudze et al., 2009). Also, greywacke was sampled from either side of

the conglomerate member and proved to be petrographically similar. This indicates there is no distinct change in the sediment composition and that the conglomerate is merely interbedded within the sequence. The conglomerate is most likely a result of short bursts of intense flooding of the river systems that carried a heavy sediment load. As a result, the rivers washed out farther into the delta system due to the increased energy. A detailed stratigraphic column (Fig. 15) has been produced showing facies variation in the greywacke sequence, focusing on the change in sedimentary features and composition.

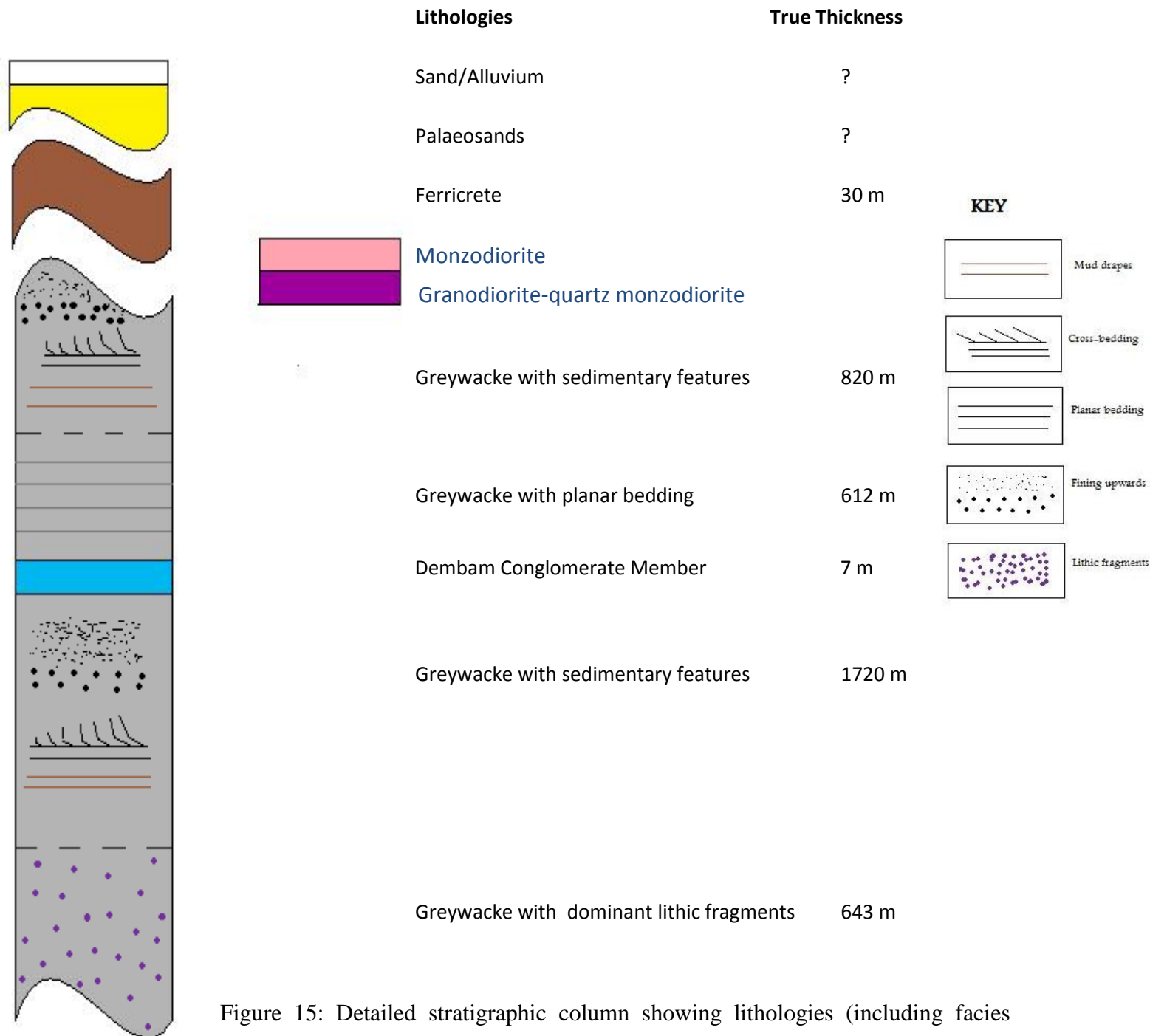


Figure 15: Detailed stratigraphic column showing lithologies (including facies variation), deformation events and true thicknesses of the units.

The stratigraphic column is important as it helps verify the depositional environment. The column attempts to characterize the greywacke in terms of different lithofacies. This was determined by slight facies changes shown by the change in prominent sedimentary features, composition changes and abundances of lithic fragments. The lower-most unit in the study area is dominated by lithic-wackes. The lithic fragments are mostly volcanoclastic in character and indicate a period where there was a high rate of erosion and rapid deposition. It was not influenced greatly by fluid flow. This is because there is a lack of sedimentary structures. The next stratigraphic unit contains sedimentary features (cross-bedding, mud drapes, gradational fining upward sequences, truncated beds, ripple marks and scour and fill structures) that indicate a shallower facies of the delta. At this point, the effects of waves and currents created cross-beds and the above mentioned sedimentary features. Gradational fining upwards sequences prevail and are intercalated with mud drapes not more than 5 cm thick. This indicates slightly calmer conditions of deposition during the cycle. The planar bedding in the unit above the conglomerate lacks shallow marine induced sedimentary features but often contain well defined beds that indicate a facies dominated by unidirectional flow. There is an overall fining upwards sequence.

9.0. Tectonic Setting

Using the sedimentary features, its composition and the type of sediments deposited, a probable basin setting can be determined. The sediments were deposited in a retro-arc basin, probably a back-arc basin. The basin was situated behind an ancient magmatic arc, which was caused by subduction. Such an extensional environment is suitable for depositing large quantities of sediment in a relatively short time (Ravanas, 1991; Ravanas and Furnes, 1995; Carter and Naish, 1998). This is synonymous with the greywacke succession of the study area which has an approximate thickness of 4.5 kilometres. Magmatic arcs are tectonically active regions with increased amounts of uplift. This results in a higher rate of erosion and therefore a higher rate of sedimentation (Boggs, 2006). The granitic clasts within the conglomerate could be sourced from the plutonic material feeding the magma chambers, which means extreme erosion must have occurred to exhume the granites. Another possibility is that the granites made up the continental crust and erosion subsequently took place during tectonically and volcanically active periods. This scenario also provides a source for the andesite, dacite and granodiorite clasts. These volcanic rocks are suggested to be the source for the greywacke in the field area and for the underlying greywackes, conglomerates and sandstone as described by Tshibubudze et al. (2009).

10.0. Discussion

The WAC, namely the Birimian Supergroup, consists of many island arc terranes that underwent terrane accretion (2300-2250 Ma). This occurred during the process of subduction, thus creating a felsic continental crust due to its association with TTG, calc-alkaline plutonism (Klein and Moura., 2009). Following this, other cratonic blocks which formed in the same way, collided with the accreted arcs to form orogenic belts and the closure of an oceanic basin. The Eburnean Orogeny is an example of this process (Hirdes et al., 1996; Hein et al., 2004; Feybesse et al., 2006). The OGGB is one of the island arc terranes, and the east Markoye region is most likely a small, but proximal to the source, portion of the back-arc basin.

Vidal et al. (2009) suggested that that the greenstone terranes of the WAC were deposited first in the stratigraphic succession between 2250-2170 Ma and occurred together with TTG plutonism. The supracrustal rocks of the OGGB that make up part of the Birimian Supergroup and overlie basement granite-adamellite (Tshibubudze and Hein, in review), were deposited in a back-arc basin environment. This is identified by the thick turbiditic greywacke sequences which are typical of arc-basin terranes. These arc terranes precede both orogenic events, i.e., The Tangaeen Event and the Eburnean Orogeny. The source of the sediments was an island arc, of an unknown, but proximal distance from the basin. The island arc would have been an area of topographical highlands. This was caused by an isostatic response to the upper plate being pushed up during subduction as the subducting plate moves down. Mountains also formed well due to the calc-alkaline plutons that develop causing uplift of the upper crust (Davis and Reynolds, 1996; Goudie, 2001). The outpour of andesite lavas and various calc-alkaline compositions, during periods of volcanism would have been responsible for extending the mountain belt upwards by constantly adding more lava. It is unknown where the magmatic arc for the basin in question was situated (Prof Ncube-Hein, pers. comms.) but based on the sedimentology and volcanoclastics of the OGGB (Tshibubudze et al., 2009; Tshibubudze and Hein, in review) an arc terrane can be interpreted as the source.

A similar, modern environment exists in the Wanganui Basin in New Zealand. The Wanganui Basin is a shallow marine environment from the Plio-Pleistocene and exhibits a full range of sedimentary facies. It is still being in-filled today with sediment from an active volcanic arc (Carter and Naish., 1998). Thick sequences of greywacke and thin conglomerate beds from the Mesozoic are deposited in the 5 km deep basin and overlie basement rocks (Proust et al., 2005). The basin is interpreted to occupy a back-arc setting today at the convergent margin of the Pacific and Australian plates, where rapid deposition has taken place due to eustatic changes (Carter and Naish., 1998). The Wanganui Basin is infilled with shales, sandstones and thick greywacke sequences with intercalated conglomerate beds. This is a good correlation to the sediments of the Birimian Supergroup and particularly the 4 km thick sequence of greywacke in the study area. It is typical for thick sedimentary sequences to be deposited during the spreading of a back-arc environment like in back-arc environments in Norway (between Solund and Bremanger) and New Zealand (Ravanas, 1991; Ravanas and Furnes, 1995; Carter and Naish., 1998).

Sediment sourced from the arc settings was transported in river systems that travelled from the uplifted regions, towards the basin. The sediment was then deposited in a deltaic system. The greywackes were deposited in this deltaic system on a steep submarine slope which allowed for rapid deposition, gravity sliding and slumping, synonymous with turbiditic flows. The erosion rate of the arc is interpreted as getting progressively slower throughout the filling of the basin. This is shown by the lower greywacke unit in the stratigraphic succession, having a much higher abundance of lithic fragments and igneous minerals compared to the overlying units. The Dembam Conglomerate Member and those described by Tshibubudze et al., (2009) lower down in the stratigraphy may have been deposited very rapidly, possibly within 1 day. Perhaps this occurred during times of flood. This negates the idea of the field area's original classification of Tarkwa Group rocks (Milesi et al., 1989, 1992). The Tarkwa Group, in the type section in Ghana overlies the Birimian supracrustal rocks unconformably. The Dembam Conglomerate Member is interbedded within greywacke from the Birimian Supergroup and does not fit the description for the Tarkwaian Group, post-orogenic molasse deposits, as described in Ghana (Milesi et al., 1991; Leube et al., 1990).

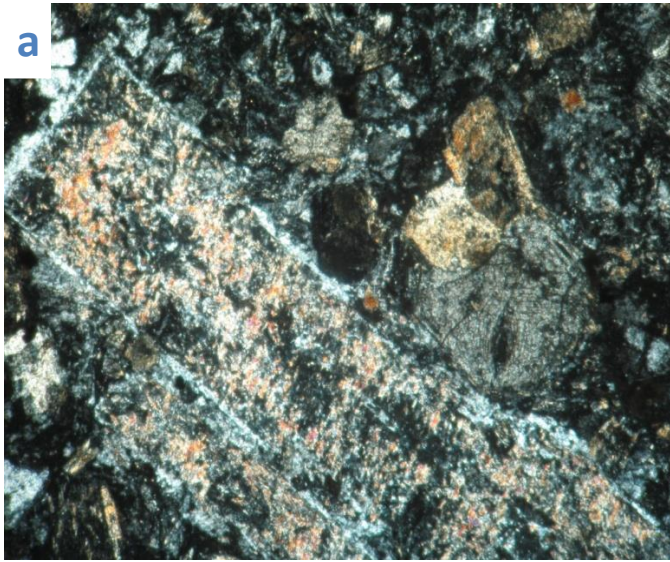
The supracrustal rocks of the Birimian Supergroup in OGGB were subsequently intruded by quartz-monzonitic, monzodioritic and granodioritic dykes and sills. They were cross-cut by northeast-trending cleavage and folds. Contact metamorphism to hornblende-hornfels facies of the country rock is also associated with these intrusions and is thus an early stage metamorphism because they are folded. Tshibubudze and Hein (in review) indicated that calc-alkaline dykes and sills are pre-D1 in age. Both the greywacke and intrusives in the field area were affected by the discreet folding of F1 and then refolded much more intensely by F2.

Associated with the Eburnean Orogeny (D2) was the emplacement of large granitoid plutons throughout the WAC (cf., Hirdes and Davis, 2002; Pawlig et al., 2006; Vidal et al., 2009; Lompo, 2009, 2010). This resulted in regional metamorphism to middle greenschist facies. This metamorphism is ubiquitous across the field area and the OGGB except in places where large granitic batholiths such as the Dori Batholith (pre-D1) intruded and metamorphic grade attain granulite facies (Tshibubudze et al., 2009; Tshibubudze and Hein, 2010). Syn-D2, N-S extensional faulting occurs throughout the belt. Dilation of the fault is a result of the maximum compressive stress in a SE-NW orientation.

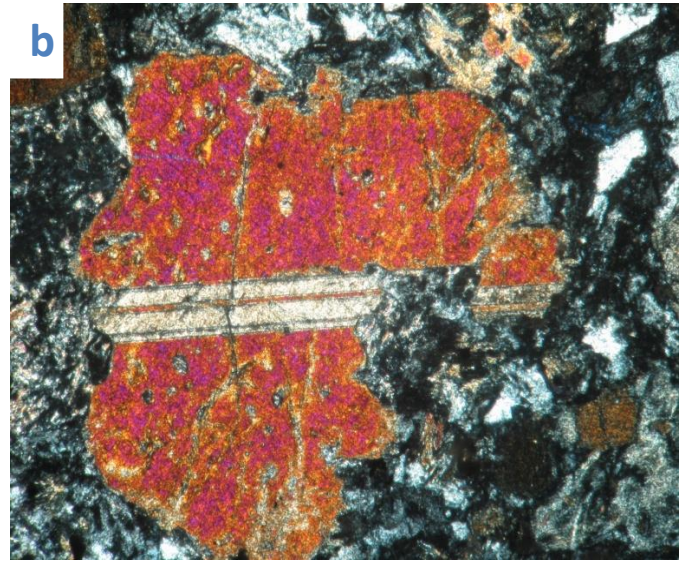
Back-arc extension and crustal thinning occurred in the OGGB. This allowed for mantle upwelling and the formation of a spreading centre. The lavas of which, correspond to the hyaloclastite basaltic pillow lavas described by Tshibubudze et al. (2009) at the base of the OGGB. With lithospheric stretching and crustal thinning, the mantle would be in close proximity to the lower crust, causing an increase in the geothermal gradient. The static, regional thermal gradient increase may have resulted in diastathermal metamorphism. Metamorphism in the OGGB most-likely continued as long as the back-arc was under extension and the mantle was closer to the crust. Because the arc-terrane were active before the Eburnean Orogeny, it suggests that metamorphism to greenschist facies in the OGGB may pre-date the orogenic event.

Ferricrete exists in the OGGB (Fig. 18) and throughout most of the WAC. It unconformably overlies the above geology. It is important stratigraphically as it is easily correlated. There is

more than a 1.9 Ga hiatus in the sedimentary sequence of the belt. This ferricrete is overlain by recent, unconsolidated aeolian sediments and alluvium which make up most of the recent stratigraphy of the OGGB. $^{39}\text{Ar}-\text{Ar}^{40}$ age dating of laterite at Tambão, north of the field area, suggested that the last period of weathering and oxidation was between 18 Ma and 3 Ma which was the time the iron-rich laterites formed (Beauvais et al., 2008). This weathering is a reworking of previously formed bauxite deposits from a tropical palaeo-climate that dominated the region approximately 60 Ma. Mechanical weathering dominated the last 18 Ma and ultimately produced the glaciis that are seen today (Beauvais et al., 2008). The laterite and ferricrete form part of the stratigraphy in the field area. It can be correlated across large areas as it represents a large gap in the stratigraphy. Palaeoproterozoic rocks are weathered to produce the iron-rich laterite which suggests that any cover rocks overlying the Birimian were subsequently eroded.



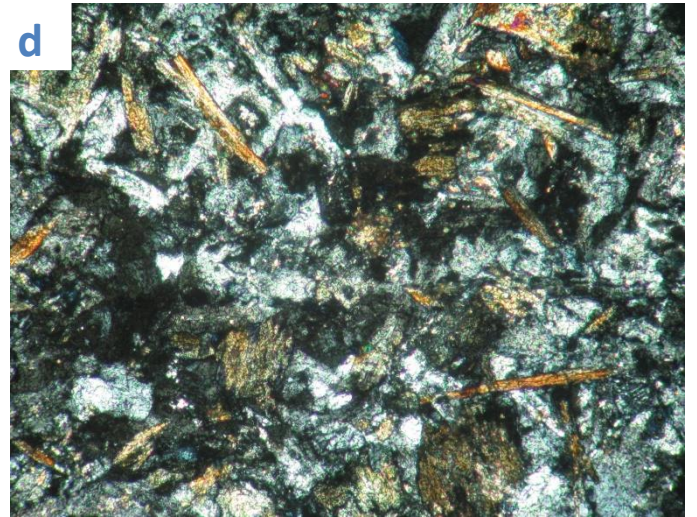
1 mm



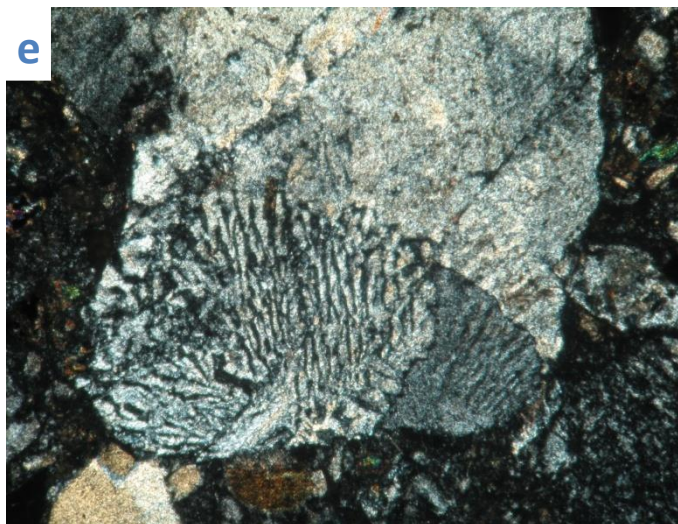
1 mm



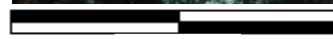
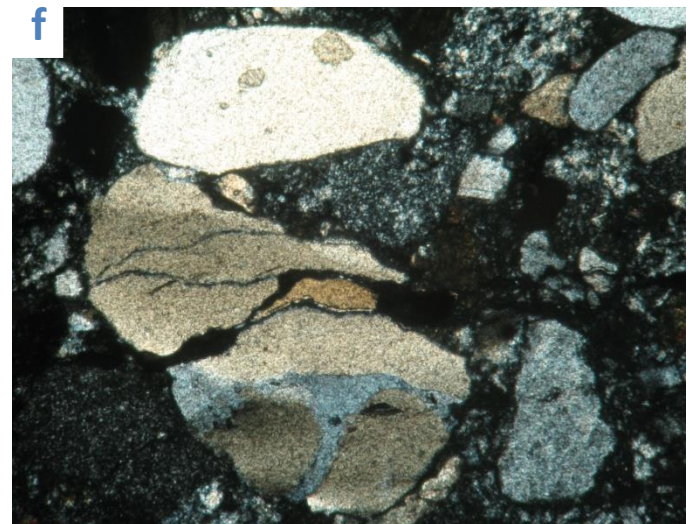
1 mm



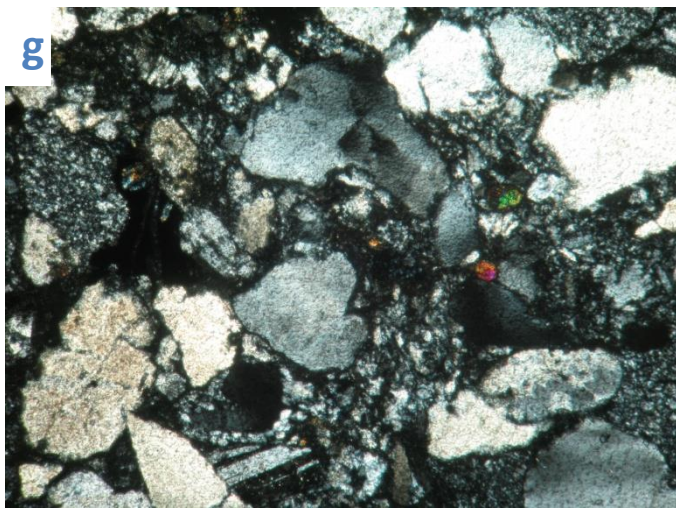
0.5 mm



1 mm



1 mm



1 mm



1 mm

Figure 16: a. *KH/LP/022*: Deuterically altered, euhedral plagioclase crystal surrounded by a groundmass of quartz, plagioclase and cpx phenocrysts. b. *KH/LP/022*: Altered, twinned cpx crystal in a groundmass of quartz, plagioclase and cpx c. *KH/LP/113*: Fine-grained hornfels greywacke-no sedimentary features visible d. *KH/LP/147*: Randomly oriented hornblende needles e. *KH/LP/065a*: Granophyric texture within a greywacke f. *KH/LP/065 b*: Larger, angular-intermediate quartz and chert grains in a matrix of smaller quartz, plagioclase and chert grains g. *KH/LP/65b*: chert, quartz, plagioclase and cpx are the most abundant minerals in the greywacke samples h. *KH/LP/114*: Large quartz and chert grains affected by ferroginisation.

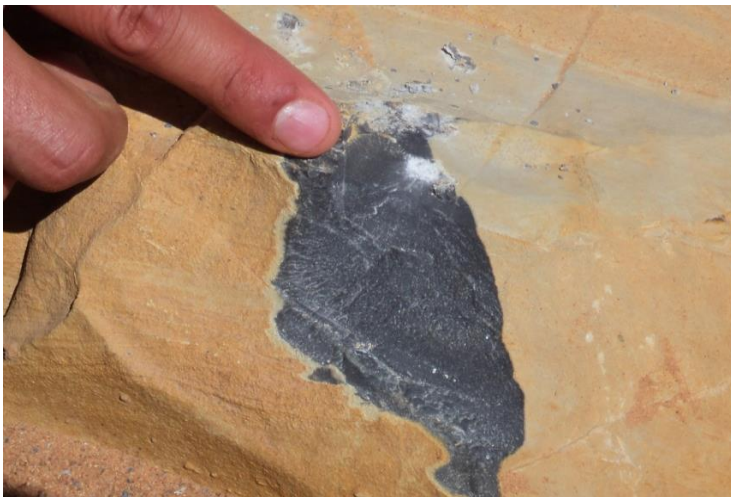


Figure 8: A bleached hornfels with no internal structure and finely grained.



Figure 6 a & b: Images showing the lack of in-situ rock and the abundance of loose boulders.



Layer A-Planar and cross-bedding

Layer B-Massive and graded

Figure 17: Layer A and B of a Bouma sequence in the greywackes

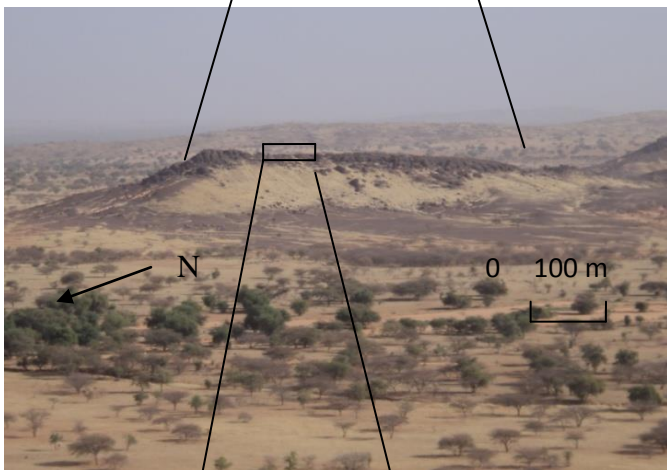
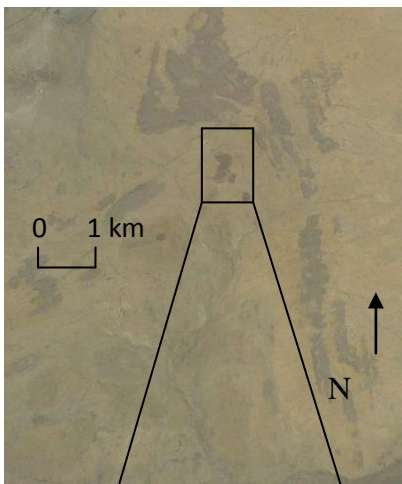


Figure 18: Laterite capped ridges covering a relatively large area of the study region.

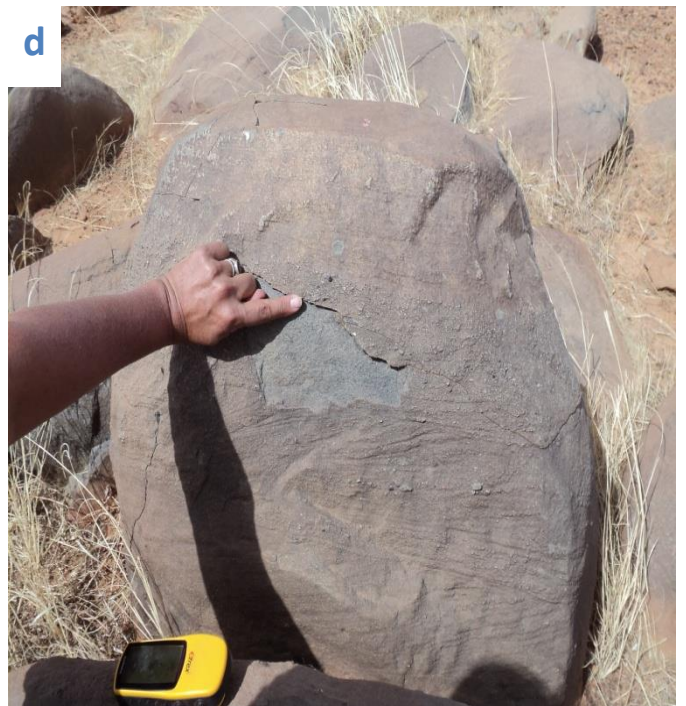
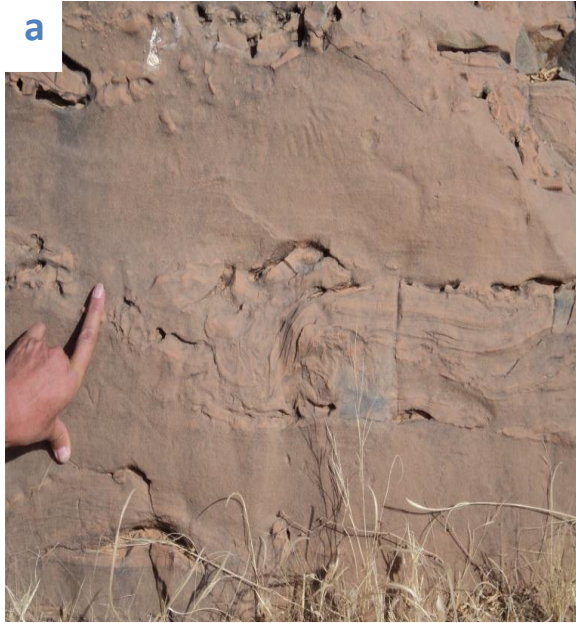




Figure 19: **a.** Polymict cobble conglomerate bed (Dembam member) with sub-angular-angular clasts of dacite, granite, metasandstone, green chert, black chert and vein quartz in a opposite directions **d.** Flame structures indicating flow direction from left to right **e.** Gravity induced slumping within greywacke **f.** Ripple marks and planar bedding



Figure 20 a,b & c: Photograph of monzodiorite - quartz monzodiorite showing elongated plagioclase crystals and a groundmass of clinopyroxene.

11.0. Conclusions

Field data and interpretation lead to the establishment of a detailed lithofacies stratigraphic section for the field area. The stratigraphy can be divided into five supracrustal lithological units; greywacke with an interbed of conglomerate, ferricrete, palaeosands and alluvium. The last two units however, make up more recent sedimentary deposits and were not given too much focus. The greywacke unit can be further sub-divided into three different facies which are defined by the sedimentary features, abundance of lithic fragments and composition. It is concluded that the rocks of that make up this stratigraphic section belong to the Birimian Supergroup. This allows for a more regional correlation of the stratigraphy. The depositional environment is recognised as a deltaic environment, with turbiditic flows within a back-arc basin of an island arc. This is due to the enormous amount of greywacke deposited, which is typical of arc basin environments.

The overall metamorphism is low-middle greenschist facies which correlates with the regional metamorphic grade in the WAC. It is a result of large, syntectonic TTG, calc-alkaline pluton emplacement. However, in the OGGB, it is proposed to be a result of earlier diastathermal metamorphism caused by crustal thinning during back-arc spreading. Contact metamorphism of the greywacke exists within a close proximity to a series of monzodiorite and granodiorite dykes that intruded the supracrustal rocks and the grade is at hornblende-hornfels facies.

The intrusive rocks are intermediate and calc-alkaline in composition and geochemically show enrichment in LREE relative to HREE and to chondrite. The monzodiorite and granodiorite dykes intruded before D1, shown by a regional cross-cutting fabric. Structurally, gentle folding occurred during D1 with compression in a NW direction occurred, followed by a much more intense, NE oriented, deformation event which refolded the rocks. This resulted in a doubly-folded sequence of asymmetrical, east-dipping, east facing anticlines and synclines. Late extensional stresses caused the Ludovic Fault System to develop. It is a series of dextral-reverse normal faults which cross-cut the entire field area. Regionally, these structural events correlate with the Tangaeen Event (D1) and the Eburnean Orogeny (D2) with the latter deforming most of the WAC.

12.0. References

Albarede, F., (2003). *Geochemistry: An Introduction*. Cambridge University Press, Cambridge, 248 pp.

Anders, E., and Grevesse, N., (1989). Abundances of the elements: Meteoric and solar. *Geochemica et Cosmochimica Acta*, **53**, 197-214.

Barker, D. S., (1970). Compositions of Granophyre, Myrmekite, and Graphic Granite. *The Geological Society of America*, **81**, 3339-3350.

Beauvais, A., Ruffet, G., Henocque, O., Colin F., (2008). Chemical and physical erosion rhythms of the West African Cenozoic morphogenesis: The ^{39}Ar - ^{40}Ar dating of supergene K-Mn oxides. *Journal of Geophysical Research*, **113**, 1-15.

Beziat, D., Dubois, M., Debat, P., Nikiema, S., Salvi, S., Tollon, F., (2008). Gold metallogeny in the Birimian craton of Burkina Faso (West Africa). *Journal of African Earth Sciences*, **50**, 215–233.

Boggs, S., (2006). *Principles of Sedimentology and stratigraphy: Fourth Edition*, Pearson Prentice Hall, New Jersey, 662 pp.

Bossiere, G., Bonkougou, I., Peucat, J. J., Pupin, J. P., (1996). Origin and age of Palaeoproterozoic conglomerates and sandstones of the Tarkwaian Group in Burkina Faso, West Africa. *Precambrian Research*, **80**, 153-172.

Bouma, A. H., (1962). *Sedimentology of some flysch deposits: A graphic approach to facies interpretation*, Elsevier, Amsterdam, 168pp.

Brown, E. T., Bourles, D. L., Colin, F., Safno, Z., Raisbeck, G. M., Yiou, F., (1994). The development of iron crust lateritic systems in Burkina Faso, West Africa examined with in-situ-produced cosmogenic nuclides. *Earth and Planetary Science Letters*, **124**, 19–33.

Burke, K., Gunnell, Y., (2008). *The African erosion surface: a continental-scale synthesis of geomorphology, tectonics, and environmental change over the past 180 million years.* Published by Geological Society of America, 34-40.

Carter, R. M. and Naish, T. R., (1998). A review of Wanganui Basin, New Zealand: global reference section for shallow marine, Plio–Pleistocene (2.5–0 Ma) cyclostratigraphy. *Sedimentary Geology*, **122**, 37-52.

Davis, D. W., Hirdes, W., Schaltegger, Nunoo, A., (1994). U–Pb age constraints on deposition and provenance of Birimian and gold-bearing Tarkwaian sediments in Ghana, West Africa. *Precambrian Research*, **67**, 89–107.

Davis, G. H., Reynolds, S. J., (1996). *Structural Geology of rocks and regions: Second edition.* John Wiley and Sons, Inc., USA, 776.

Dott, R. H., (1964). Wacke, Graywacke and matrix-what approach to immature sandstone classification? *Journal of Sedimentary Petrology*, **34**, 625-632.

Feybesse, J.-L., Milesi, J.-P., Ouedraogo, M.F., Prost, A., (1990). La “ceinture” Proterozoïque inférieure de Boromo–Goren (Burkina Faso): un exemple d’interférence entre deux phases transcurrentes éburnéennes. *Comptes Rendus de l’Académie des Sciences de Paris, Série II, Sciences de la Terre et des Planètes*, **310**, 1353–1360.

Feybesse, J. L., Billa, M., Guerrot, C., Duguey, E., Lescuyer, J. L., Milesi, J. P., Bouchot, V., 2006. The paleoproterozoic Ghanaian province: geodynamic model and ore controls, including regional stress modelling. *Precambrian Research*, 149–196.

Fischer, R. V., Schmincke, H. U., (1994). Volcaniclastic sediment transport and deposition. In: Pye, K. (Ed.), *Sediment transport and depositional processes*. Blackwell Scientific Publishing, London, 351-388.

Furnes, H., Ravanás, R., (1995). The use of geochemical data in determining the provenance and tectonic setting of ancient sedimentary successions: the Kalvag Melange, western Norwegian Caledonides. In: Plint A. G. (Ed.), *Sedimentary Facies Analysis: A tribute to the research and teaching of Harold G. Reading*. Blackwell Publishing, Oxford, 237-264.

Goudie, A., (2001). *The nature of the environment: 4th Edition*. Blackwell Publishers Ltd, Oxford, 544 pp.

Harcöuet, V., Guillou-Frottier, L., Bonneville, A., Bouchot, V., Milesi, J. P., (2007). Geological and thermal conditions before the major Palaeoproterozoic gold mineralization event at Ashanti, Ghana, as inferred from improved thermal modelling. *Precambrian Research*, **154**, 71–87.

Hein, K. A. A., (2003). Relative timing of deformational, metamorphic and mineralisation events at the Mt. Todd (Yimuyun Manjerr) Mine, Pine Creek Inlier, Northern Territory, Australia. *Ore Geology Reviews*, **22**, 143-175.

Hein, K. A. A., Morel, V., Kagone, O., Kiemde, F., Mayes, K., (2004). Birimian lithological succession and structural evolution in the Goren Segment of the Boromo-Goren Greenstone Belt, Burkina Faso. *Journal of African Earth Sciences*, **39**, 1–23.

Hein, K. A. A., (2010). Succession of structural events in the Goren greenstone belt (Burkina Faso): Implications for West African tectonics. *Journal of African Earth Sciences*, **56**, 83-94.

Hein, K.A.A., Matabane, M.R., in review . The gold-bearing intrusion-related deposits of the FE3 opencast gold mines, Sadiola goldfield, Kedougou-Kéniéba Inlier, western Mali. *Ore Geology Reviews*.

Hirdes, W., Davis, D. W., Eisenlohr, B. N., (1992). Reassessment of Proterozoic granitoid ages in Ghana on the basis of U/Pb zircon and monazite dating. *Precambrian Research*, **56**, 89-96.

Hirdes, W., Davis, D. W., Ludtke, G., Konan, G., (1996). Two generations of Birimian (Paleoproterozoic) volcanic belts in north-eastern Cote d'Ivoire (West Africa): consequences for the Birimian controversy'. *Precambrian Research*, **80**, 173–191.

Junner, N.R., (1935). Gold in the gold coast, Ghana Geological Survey Memoir, No. 4, 67pp.

Hirdes, W., Davis, D. W., (2002). U-Pd geochronology of Palaeoproterozoic rocks in the southern part of the Kedougou-Kenieba Inlier, Senegal, West Africa: Evidence for diachronous accretionary development of the Eburnean province. *Precambrian Research*, **118**, 83-99.

Klein, E.L., Moura, C.A.V., (2009). São Luis craton and Gurupi belt (Brazil): possible links with the West African craton and surroundings Pan-African belts. In: Pankhurst, R.J., Trouw, R.A.J., Britto Neves, B.B., de Wit, M.J. (Eds.), *West Gondwana: Pre-Cenozoic correlations across the South-Atlantic region*, Geological Society, London, 137–151 (Special Publications).

Le Maitre, R.W., Bateman, P., Dudek, A., Keller, J., Lameyre, J., Le Bas, M. J., Sabine, P. A., Schmid, R., Sorensen, H., Streckeisen, A., Woolley, A. R., Zanettin, B., (1989). *A Classification of Igneous Rocks and Glossary of terms: Recommendations of the International Union of Geological Sciences Subcommittee on the Systematics of Igneous Rocks*. Blackwell Scientific Publications, Oxford, U.K. 236 pp.

Leube, A., Hirdes, W., Mauer, R., Kesse, G. O., (1990). The early Proterozoic Birimian Supergroup of Ghana and some aspects of its associated gold mineralization. *Precambrian Research*, **46**, 139–165.

Lompo, M., (2009). Geodynamic evolution of the 2.5-2.0 Ga Palaeoproterozoic magmatic rocks in the Leo-Man Shield of the West African Craton. A model of subsidence of an oceanic plateau. In: Reddy, S. M., Mazumder, R., Evans, D. A. D., Collins, A. S. (Eds.), Palaeoproterozoic and global evolution. Geological Society, London, Special Publication 323, 231-254.

Lompo, M., (2010). Palaeoproterozoic structural evolution of the Man-Leo Shield (West Africa). Key structures for vertical to transcurrent tectonics. *Journal of African Earth Sciences*, **58**, 19–36.

Milesi, J. P., Feybesse, J. L., Ledru, P., Dommaget, A., Ouedraogo, M. F., Marcoux, E., Prost, A., Vinchon, Ch., Sylvain, J. P., Johan, V., Tegye, M., Calvez, J. Y., Lagny, P., (1989). West African gold deposits, in their lower Proterozoic lithostructural setting. *Chronique de la Recherche Minière*, **497**, 3–98.

Milesi, J.P., Ledru, P., Ankrah, P., Johan, V., Marcoux, E., Vinchon, C., (1991). The metallogenic relationship between Birimian and Tarkwaian gold deposits in Ghana. *Mineralium Deposita*, **26**, 228–238.

Milesi, J.P., Ledru, P., Feybesse, J.L., Dommaget, A., Marcoux, E., (1992). Early Proterozoic ore deposits and tectonics of the Birimian orogenic belt, West Africa. *Precambrian Research*, **58**, 305–344.

Needham, R. S., Stuart-Smith, P. G., Page, R. W., (1988). Tectonic evolution of the Pine Creek Inlier, Northern Territory. *Precambrian Research*, **40/41**, 543-564.

Nesse, W. D., (2000). Introduction to mineralogy. Oxford University Press, Oxford, pg 92, 442 pp.

Neuerburg, G. J., (1958). Deuteric alteration of some aplite-pegmatites of the Boulder Batholith, Montana, and its possible significance to ore deposition. *Economic Geology*, **53**, 287-299.

Pawlig, S., Gueye, M., Klischies, R., Schwarz, S., Wemmer, K., Siegesmund, S., (2006). Geochemical and Sr–Nd isotopic data on the Birimian of the Kedougou-Kenieba Inlier (Eastern Senegal): implications on the Palaeoproterozoic evolution of the West African Craton. *South African Journal of Geology*, **109**, 411–427.

Proust, J. N., Lamarche, G., Nodder, S., Kamp, P. J. J., (2005). Sedimentary architecture of a Plio-Pleistocene proto-back-arc basin: Wanganui Basin, New Zealand. *Sedimentary Geology*, **181**, 107-145.

Ravanas, R., (1991). A sedimentological, geochemical and provenance study of the Kalvag Melange, western Norwegian Caledonides, Thesis (unpublished). University of Bergen, 212 pp.

Shanmugam, G., (1997). The Bouma sequence and the turbidite mindset. *Earth Science Reviews*, **42**, 201-229.

Streckeisen, A. L., (1976). To each plutonic rock its proper name. *Earth-Science Reviews*, **12**, 1-33.

Tshibubudze, A., Hein, K. A. A., Marquis, P., (2009). The Markoye Shear Zone in NE Burkina Faso. *Journal of African Earth Sciences*, **55**, 245–256.

Tshibubudze, A., Hein, K.A.A., in review. Structural setting of gold deposits in the Oudalan-Gourouol greenstone belt east of the Markoye Shear Zone, West African craton. *Precambrian Research*.

Vidal, M., Gumaix, C., Cagnard, F., Pouclet, A., Ouattara, G., Pichon, M., (2009).

Evolution of a Paleoproterozoic “weak type” orogeny in the West African Craton (Ivory Coast). *Tectonophysics*, **477**, 145–159.

Vernon, R. H., Clarke, G. L., (2008). *Principles of metamorphic geology*. Cambridge University Press, Cambridge, 446.

13.0. Appendix

Chondrite Values:

Sc	34.20
V	293.00
Cr	13400.00
Co	2250.00
Ni	49300.00
Cu	522.00
Zn	1260.00
Ga	37.80
Rb	7.09
Sr	23.50
Y	4.64
Zr	11.40
Nb	0.69
Mo	2.55
Ba	4.49
Pb	3.15
Th	0.03
U	0.01
La	0.45
Ce	1.14

Pr	0.17
Nd	0.83
Sm	0.26
Eu	0.10
Gb	0.33
Td	0.06
Dy	0.39
Ho	0.09
Er	0.25
Tm	0.04
Yb	0.25
Lu	0.04

(Anders and Grevesse, 1989).

ICP-MS Data

ppm	LP145	LP147	LP148
Li	21.948	25.259	18.112
Ga	17.387	16.819	16.577
Sn	2.53	4.823	1.578
Cs	2.696	1.689	3.783
La	31.323	24.864	25.752
Ce	72.779	55.16	64.069
Pr	6.599	5.467	5.339
Nd	22.196	18.908	19.298
Sm	3.774	3.509	3.336
Eu	0.817	0.931	0.79
Gd	3.06	2.712	2.678
Tb	0.465	0.421	0.406
Dy	3.16	2.777	2.834
Ho	0.693	0.583	0.607

Er	1.96	1.637	1.763
Tm	0.3	0.243	0.279
Yb	2.178	1.801	2.022
Lu	0.344	0.283	0.332
Hf	6.334	4.659	6.059
Ta	0.761	0.504	0.706
W	0.25	0.888	0.196
Pb	10.621	9.087	10.932
Th	7.344	5.252	6.435
U	2.535	1.963	2.456

(Courtesy of the Earth Lab, University of the Witwatersrand)

XRF Data

Majors:

	KH/LP/145	KH/LP/147	KH/LP/148
SiO ₂	69.03	63.16	69.53
TiO ₂	0.4659	0.5801	0.4325
Al ₂ O ₃	15.03	14.97	14.79
Fe ₂ O ₃	0.38	0.64	0.36
FeO	3.07	5.2	2.93
MnO	0.07	0.12	0.07
MgO	1.37	3.46	1.29
CaO	2.62	5.68	2.85
Na ₂ O	3.83	3.47	3.92
K ₂ O	3.48	2.48	3.47
P ₂ O ₅	0.16	0.19	0.15
TOTAL	99.49	99.97	99.8
LOI	1.18	1.77	1.73

(Courtesy of the Earth Lab, University of the Witwatersrand)

Traces:

		KH/LP/148	KH/LP/147	KH/LP/145
Sc	(ppm)	6.61	18.69	8.07
V	(ppm)	51.33	128.38	56.97
Cr	(ppm)	12.35	97.8	25.16
Co	(ppm)	7.54	21.65	11.14
Ni	(ppm)	7.85	21	9
Cu	(ppm)	8.26	20.93	4.65
Zn	(ppm)	44.93	54	48.63
Ga	(ppm)	16.2	15.68	15.77
Rb	(ppm)	117.88	84.98	113.51
Sr	(ppm)	343.89	448.87	339.29
Y	(ppm)	18.58	13.28	18.29

Zr	(ppm)	154.93	110.31	145.3
Nb	(ppm)	7.25	5.75	7.37
Mo	(ppm)	0.85	1.51	1.7
Ba	(ppm)	621.54	478.52	604.32
Pb	(ppm)	12.49	6.65	10.75
Th	(ppm)	8.53	6.39	7.79
U	(ppm)	4.76	0.97	3.24

(Courtesy of the Earth Lab, University of the Witwatersrand)